AIAA SciTech Forum
23-27 January 2023, National Harbor, MD & Online
AIAA SCITECH 2023 Forum

10.2514/6.2023-1686

# Uncertainty Propagation in High-Dimensional Fields using Non-Intrusive Reduced Order Modeling and Polynomial Chaos

Nikhil Iyengar*, Dushhyanth Rajaram†, Kenneth Decker‡, and Dimitri Mavris§
*Aerospace Systems Design Laboratory, Georgia Institute of Technology, Atlanta, GA, 30332 USA*

**High-fidelity, physics-based modeling and simulation have become integral to the design of aircraft, but can have intractably high computational costs when used for uncertainty quantification. This study presents a non-intrusive, parametric reduced order modeling method to enable the prediction of uncertain high-dimensional outputs with complex, nonlinear features and limited sampling budgets. A Proper Orthogonal Decomposition (POD) procedure is utilized to reduce the dimensionality of the high-dimensional space and identify a low-dimensional latent space. A sparse regression-based polynomial chaos expansion (PCE) is then used to construct a mapping between the uncertain input parameters and the latent space coordinates. The methodology is assessed on three test cases, including two-dimensional transonic flow around the RAE2822 airfoil with geometric uncertainties and several canonical problems with varying input and output space dimensionality. The study focuses on problems with strong nonlinearities and discontinuities, such as shocks, to investigate the effectiveness of the ROM in predicting high-speed aerodynamic fields. The performance is assessed by comparing the uncertain mean, variance, point predictions, and integrated quantities of interest obtained using the ROMs to Monte Carlo simulations.**

## NOMENCLATURE

| | | |
|---|---|---|
| $\mathcal{M}$ | = | Computational model |
| $C_p$ | = | Pressure coefficient |
| $a$ | = | PCE coefficients |
| $b$ | = | Number of design variables |
| $d$ | = | ROM dimension |
| $e$ | = | Relative error |
| $g$ | = | Generic functions |
| $i, j, k, l$ | = | Generic indices |
| $n$ | = | Dimension of the high-fidelity fields |
| $M$ | = | Mach number |
| $m$ | = | Number of training snapshots |
| $P$ | = | PCE truncation rank |
| $v$ | = | Number of validation snapshots |
| $w$ | = | Weight coefficients |
| $\boldsymbol{X}$ | = | Matrix of high-fidelity snapshots |
| $\boldsymbol{x}$ | = | Single high-fidelity snapshot |
| $\mathbf{y}$ | = | High-fidelity uncertain snapshot |
| $\boldsymbol{Z}$ | = | Matrix of high-fidelity points projected on latent space |
| $\boldsymbol{z}$ | = | Coordinates of single high-fidelity point in latent space |
| $\alpha$ | = | PCE basis order |
| $\beta$ | = | Shock angle |
| $\theta$ | = | Generic angle |
| $\boldsymbol{\xi}$ | = | Vector of random inputs |

*Ph.D. Candidate, School of Aerospace Engineering (ASDL), Georgia Tech, Student AIAA Member
†Research Engineer II, School of Aerospace Engineering (ASDL), Georgia Tech, AIAA Member
‡Research Engineer, School of Aerospace Engineering (ASDL), Georgia Tech, AIAA Member
§S.P. Langley Distinguished Regents Professor and Director of ASDL, Georgia Tech, AIAA Fellow

| | | |
|---|---|---|
| $\sigma$ | = | Singular value |
| $\phi$ | = | POD mode |
| $\Phi$ | = | Matrix of POD modes |
| $\psi$ | = | PCE polynomial |
| $\Psi$ | = | Matrix of PCE polynomials |
| $\Omega$ | = | Computational domain |

| | | |
|---|---|---|
| *CFD* | = | Computational Fluid Dynamics |
| *DOE* | = | Design of Experiments |
| *DR* | = | Dimensionality Reduction |
| *DV* | = | Design Variable |
| *FFD* | = | Free-Form Deformation |
| *FOM* | = | Full Order Model |
| *HF* | = | High-fidelity |
| *MC* | = | Monte Carlo |
| *LHS* | = | Latin Hyper Sphere |
| *PCE* | = | Polynomial Chaos Expansion |
| *PDF* | = | Probability Density Function |
| *POD* | = | Proper Orthogonal Decomposition |
| *RANS* | = | Reynolds Average Navier-Stokes |
| *RIC* | = | Relative Information Content |
| *ROM* | = | Reduced Order Model |
| *SVD* | = | Singular Value Decomposition |
| *QoI* | = | Quantity of Interest |
| *UQ* | = | Uncertainty Quantification |



# I. Introduction

The design of novel aircraft relies extensively on the use of physics-based models and simulations as historical data is limited, restricted, or not comprehensive. In fact, today, as these tools have been shown to provide realistic estimations of system behavior and performance at a significantly lower computational cost compared to physical experiments [1], they have become a central component during design.

During the traditional aircraft design process, practitioners can rely on integrated (scalar) quantities of interest (QoI) to guide decision making. For example, the lift coefficient, drag coefficient, wing loading, and take-off gross weight are some of the most prominent scalar quantities that provide aggregate performance information. On the other hand, during the design of novel aircraft, it important to know the spatial (and perhaps temporal) *distribution* of quantities around an aircraft to guide decision making. The term "field" is often used to describe this distribution of information. Take, for example, the supersonic business jet, where changes in aircraft geometry, flight conditions, and atmosphere significantly impact the aerodynamic field around the body. This field is characterized by several nonlinear, discontinuous features, such as shockwaves and expansion fans. The strength, location, shape, and size of these features must be known precisely for downstream disciplinary analysis, such as structural optimization, aeroelastic performance estimation, and shape optimization.

Often, due to variation in the manufacturing process, atmosphere, and flight conditions, there is uncertainty in the performance of the aircraft. The sensitivities of performance metrics to uncertain parameters can be used to determine where research, time, and capital should be spent to improve system robustness. The identification, characterization, propagation, and mitigation of these uncertainties in simulations and experiments is referred to as uncertainty quantification (UQ).

An essential part of uncertainty propagation is determining the distribution of outputs due to variations in inputs and obtaining estimates for the expected value (first order statistical moment) and variance (second order statistical moment). Monte Carlo (MC) methods are the benchmark for UQ and perform a random sampling of the uncertain input space and propagate it through the full-order model (FOM) to get output distributions. It can be shown that the error estimate for Monte Carlo has slow convergence and drops with a rate of $O(1/\sqrt{m})$, where $m$ is the number of samples. Thus, for computationally expensive analyses, where the sampling budget is limited, only rough estimates for statistics can be

obtained. When coupled with high-fidelity numerical simulations, MC methods can lead to intractable computational costs and has imposed practical constraints on their use in UQ.

### A. Surrogate Modeling

One common approach to performing UQ with expensive tools is to reduce the number of samples by neglecting certain variables. For example, in [2], the authors perform a sensitivity analysis of uncertain inputs with high-fidelity analyses, but, based on prior knowledge, neglect certain variables to reduce the overall simulation load. However, if the system's dynamics are not fully understood, researchers cannot simply neglect variables without losing valuable insight. Alternatively, some researchers have relied on adjoint-based methods which give analytical equations to calculate the derivatives (or sensitivities) of an output with respect to input variables. This allows for efficient calculation of design sensitivity for even a large number of design variables [3]. However, the most significant hurdle to adjoint-based analysis is that they require access to the governing equations, lengthy modifications to the full-order model (FOM) code to create and/or verify adjoint calculations, and, sometimes, are impossible to derive. Methods which require such modifications and access to the numerical simulation tool's code are referred to as *intrusive methods*. This is challenging because the implementation details of many software packages are often proprietary and inaccessible to the user for modification. As such, this study focuses on non-intrusive methods for UQ.

The deficiencies of the aforementioned methods and the excessive computational cost of expensive simulations led to the development of surrogate models. Surrogate models have been used in a wide array of contexts with several survey papers outlining the current state-of-the-art [4–6]. While there exist several varieties of surrogate modeling methods for UQ, Gaussian Process Regression (GPR), closely related to Kriging, and Polynomial Chaos Expansion (PCE) have received much attention lately. GPR is an interpolation routine that incorporates prior knowledge about a functional relationship [7]. The primary advantage of a GPR is that it excels when data is sparse and is amenable to be retrained rapidly as new data is provided. A survey of GPR for UQ is provided in [8].

Polynomial chaos relies on a pre-defined, set of orthogonal basis functions to express a output random variable by separating its deterministic and stochastic contributions. By construction, PCE offers some powerful mathematical properties:

- PCE is based on a strong mathematical foundation of probability theory, and provides guarantees on convergence rates for the surrogate model error [9–12].
- The coefficients of a PCE can be used in analytical formulas to get statistical moments and sensitivity indices (such as Sobol indices) without the need to use MC. This not only reduces the additional cost of sampling, but also prevents the accumulation of additional errors from the finite sampling of surrogates [13].
- PCE is amenable to sparse modelling, and thus can be used with limited sampling budgets when desired [14].

For these reasons, PCE will be used for handling uncertainties in this study.

### B. Challenges in High-Dimensional Problems

PCE models can be decomposed into three categories: scalar models, multi-fidelity models, and reduced order models. Scalar PCE models are trained using pairs of inputs-outputs to generate regression-based approximations of out-of-sample points. Scalar PCE models have proven to be a robust tool for UQ and used in multiple disciplines, including computational doismetry [15], dam simulations [16], and aerodynamics [17–19]. Multi-fidelity (MF) models attempt to combine data from lower-fidelity models with higher-fidelity models to reduce overall training cost but maintain predictive accuracy [6]. Recently, West et al. have investigated the performance of MF PCE models in predicting the (scalar) sonic boom loudness metric from a supersonic aircraft in uncertain flight conditons [19, 20]. While their work showed a significant computational cost reduction compared to a single-fidelity scalar PCE model, it was restricted to scalar outputs as well.

The prediction of uncertain field quantities, such as the lift distribution over a wing or pressure distribution over an airfoil, is, however, quite challenging. This is because each solution consists of perhaps millions of scalar random variables, each associated with some spatial location and having some inherent coherence dictated by the physics of the problem. Scalar models are typically inadequate for such tasks, but some researchers have resorted to applying scalar models on each node in the computational mesh, effectively generating an ensemble of scalar predictors (see [17, 21]). This process is not only expensive to perform, but also leads to extremely high storage (memory) requirements. Most important, because scalar models have no mechanism to ensure the underlying model physics, the solutions obtained may lack the spatial coherence inherent between nodes. To address this challenge, recent studies have identified full field surrogate models or Reduced Order Models (ROMs) as a key enabler for leveraging high-fidelity numerical simulations

during UQ [22].

### C. Reduced Order Models for Uncertainty Quantification

ROMs are a key enabler for leveraging rapidly growing volumes of data and bringing high-fidelity numerical simulation data earlier into the design process in a computationally efficient manner [23]. The key idea behind ROM is that the fundamental features of the high-dimensional problem can be captured using some low-dimensional subspace. A ROM attempts to identify this low-dimensional subspace and uses it to predict the high-dimensional solution for points outside the training data set at a low computational cost [22]. In doing so, ROMs retain the underlying structure of the model so spatial coherence can be maintained. Furthermore, because ROMs approximate the field, it is possible obtain all integrated QoIs that would otherwise have been modeled using numerous individual scalar surrogates. Just within aerodynamics, deterministic ROMs have been used in various problems, including subsonic, turbulent flow around cylinders [24], transonic flows past airfoils [25], and supersonic flows in nozzles [26], and hypersonic flows around blunt bodies [27].

Due to its simplicity, the Proper Orthogonal Decomposition (POD) method has been used extensively in the ROM field and, in the past decade, become prevalent in the uncertainty quantification field as well. In 2015, Raisee et. al [28] developed a POD-based method motivated by the high computational cost of training global PCE expansions in high-dimensional spaces (see the next section for a review of PCE theory). This method relies on the use of two meshes: a coarse mesh with provides a computationally efficient, albeit slightly inaccurate solution to the problem being analyzed; and a fine mesh, which is more expensive to solve, but accurately captures all the necessary features of the problem. The central assumption inherent in this method is that the POD modes identified on the coarse mesh accurately capture the dynamics in the fine mesh. This assumption requires that the coarse mesh have a high enough grid fineness that the essential features of the problem are captured. As noted by Abraham et al, the definition of a coarse mesh is a challenging task, and requires additional computational effort and/or some expert knowledge [29]. Moreover, while this method can achieve a computational cost reduction of 88% compared to a full PCE expansion on the fine mesh, it still relies on fitting scalar surrogates at each node. Indeed, this reduces the method to a variant of a scalar surrogate model and introduces possible inconsistencies in spatial coherence [21].

Alternatively, other researchers have relied on using POD to perform a dimension reduction and then constructing PCE models in the latent space. This method, called POD-PCE, bypasses the need for individual scalar models at each node and has been used in several recent papers. For example, Li et al. [30] use this method to predict the flow in the Gulf of Mexico due to uncertainties in wind conditions. Other authors have applied the POD-PCE method to acoustics [31], urban drainage simulations [32], and dynamical systems [33]. In all these papers, the researchers either work with functions which vary smoothly with random inputs or restrict their scope to mathematical benchmark problems [33]. Thus, the combined use of POD and, more generally, ROMs with PCE has been relatively unexplored in complex high-dimensional problems, such as those seen in aerodynamics, and will be further investigated in this study.

### D. Contributions of the Paper and Structure

Since the early 2000s, the PCE method has been used extensively and thoroughly investigated in a variety of uncertainty quantification problems with scalar outputs. However, current state-of-the-art scalar PCE models, even after modification to reduce sampling requirements, cannot adequately predict high-dimensional random variables.

This study focuses primarily on aerodynamic problems generated using CFD simulations, which are not amenable to traditional Monte Carlo analysis. In fact, the problems tackled in this study are specifically designed to resemble those seen in supersonic and transonic aircraft design where aerodynamic solutions can have millions of dimensions and several localized nonlinear, discontinuous features, such as shocks. The goal of this work is to investigate and quantify the ability of ROM methods to accurately and efficiently predict uncertain flow fields. In particular, this paper utilizes POD to reduce the dimensionality of the high-dimensional space and PCE for latent space regression to create a parametric, non-intrusive, computationally cheap method for UQ. As previous literature has been restricted to either scalar PCE models or linear canonical applications, this will provide empirical insight into the performance of the POD-PCE method in nonlinear high-dimensional problems seen in the design process. Further, the paper will evaluate the predictive performance of analytical PCE methods in capturing the high-dimensional mean, variance, and field distributions at unseen parameter points. Finally, the paper compares the performance of a sparse PCE procedure to a standard regression-based PCE model. The behavior of the proposed ROM method is evaluated by performing a thorough empirical assessment on three test cases, including a transonic CFD application problem. Guided by the conclusions from these experiments, this study will not only provide novel insight for the ROM and UQ field, but also

contribute to the development of methods for robust aircraft design.

The structure of the manuscript is as follows: Section II presents an overview of POD and PCE methods. Section III provides details of the proposed uncertain ROM methodology and error metrics. Section IV describes the numerical experiments and results for three test cases: uncertain flow through a converging diverging nozzle, a function resembling supersonic flow over a 2D wedge with geometric uncertainties, and uncertain flow over an RAE2822 airfoil. Section V summarizes the findings and recommendations for future work.

## II. Reduced Order Modeling

This section provides an overview of the theoretical and implementation details for the Proper Orthogonal Decomposition (POD) and Polynomail Chaos Expansion (PCE) method.



### A. Proper Orthogonal Decomposition

Due to its simplicity and versatility, for decades, the POD method has been used commonly not only in aerospace applications, but also in many other fields, such as computer science [34]. Though it is often referred to as POD in ROM literature, it is also known as Principal Component Analysis (PCA) or Karhunen-Loève Decomposition. The central idea behind POD is to identify a subspace spanned by a set of vectors that captures the most variance within a given data set. The identification of these vectors, referred to as POD modes, involves the Singular Value Decomposition (SVD) algorithm and therefore results in a linear dimensionality reduction procedure. Once an appropriate latent space is identified, the high-dimensional solution for an unseen set of parameters can be predicted at a fraction of the computational cost.

To begin, let $\mathcal{M}$ represent a deterministic model which acts on a set of inputs and yields some vector output. That is, for a given set of inputs, the computational model outputs the same values and is not itself stochastic. Let $\boldsymbol{\xi}$ represent a vector of random variables that determines the output, $\boldsymbol{x}$. Consider a matrix $\mathbf{X}$ that is composed of $m$ samples, or *snapshots*, of a field of dimension $n$ obtained from $\mathcal{M}$, such that $\mathbf{X} = \left[\mathbf{x}_1, ..., \mathbf{x}_m\right] \in \mathbb{R}^{n\times m}$. For convenience and without loss of generality, assume the matrix $\mathbf{X}$ has been mean-centered as a pre-processing step such that

$$\bar{\mathbf{x}} = \frac{1}{m}\sum_{j}^{m} \mathbf{x}_j = 0 \tag{1}$$

The Singular Value Decomposition procedure is applied to the snapshot matrix to yield:

$$\boldsymbol{X} = \boldsymbol{U}\boldsymbol{\Sigma}\boldsymbol{V}^T \tag{2}$$

where $\boldsymbol{U} \in \mathbb{R}^{n\times n}$ is the matrix of POD modes, $\boldsymbol{V} \in \mathbb{R}^{m\times m}$ is a matrix of right singular vectors, and $\boldsymbol{\Sigma} \in \mathbb{R}^{n\times m}$ is a diagonal matrix of singular values, such that $\sigma_1 \geq \sigma_2 \geq ... \geq \sigma_r \geq 0$ and $r = \min(n, m)$. The modes obtained from POD are uncorrelated (orthogonal) and maximize the variance captured from the original data [35]. To reduce the dimensionality of the problem, it is important to identify those POD modes that capture most of the dynamics. This can be done by analyzing the singular values for each POD mode and the relative information content metric:

$$RIC(d) = \frac{\sum_{i=1}^{d}\sigma_i^2}{\sum_{j=1}^{r}\sigma_j^2} \tag{3}$$

The RIC is used to describe the amount of variance that is captured by the $d$ most dominant modes. Most often, the practitioner sets the RIC to some $\delta \in [0, 1]$, then selects $d$ basis vectors such that $RIC(d) \geq \delta$, with values of $\delta \geq .9999$ seen commonly in application [36].

Once truncated, construct the matrix $\boldsymbol{\Phi}$ such that its columns consist of the $d$ orthonormal modes, $\boldsymbol{\Phi} = \left[\boldsymbol{\phi}_1, ..., \boldsymbol{\phi}_d\right] \in \mathbb{R}^{n\times d}$, where $d$ is the rank of the orthonormal basis and thus the dimension of the latent space. In statistics and computer science, when the objective is to simply identify a lower-dimensional space, the POD procedure is complete at this point. In parametric reduced order modeling though, the ROM is used to replace the FOM during the online phase. To do so, each snapshot, must first be projected onto the latent space:

$$\boldsymbol{Z} = \boldsymbol{\Phi}^T\boldsymbol{X} \tag{4}$$

where $\boldsymbol{Z}$ is the matrix whose columns correspond to each snapshot's coordinates in the latent space, such that $\boldsymbol{Z} = [z_1, ..., z_m] \in \mathbb{R}^{d\times m}$. Each $z$ is then paired with its associated set of input parameters, $\boldsymbol{\xi}$, which were used to sample

**Table 3 Askey scheme of polynomials and their links to common PDFs.**

| Distribution | Density function | Polynomial | Weight function | Support range |
|---|---|---|---|---|
| Normal | $\frac{1}{\sqrt{2\pi}}e^{\frac{-x^2}{2}}$ | Hermite $He_n(x)$ | $e^{\frac{-x^2}{2}}$ | $[-\infty,\infty]$ |
| Uniform | $\frac{1}{2}$ | Legendre $P_n(x)$ | 1 | $[-1,1]$ |
| Beta | $\frac{(1-x)^\alpha(1+x)^\beta}{2^{\alpha+\beta+1}B(\alpha+1,\beta+1)}$ | Jacobi $P_n^{(\alpha,\beta)}(x)$ | $(1-x)^\alpha(1+x)^\beta$ | $[-1,1]$ |
| Exponential | $e^{-x}$ | Laguerre $L_n(x)$ | $e^{-x}$ | $[0,\infty]$ |
| Gamma | $\frac{x^\alpha e^{-x}}{\Gamma(\alpha+1)}$ | Generalized Laguerre $L_n^{(\alpha)}(x)$ | $x^\alpha e^{-x}$ | $[0,\infty]$ |

the FOM. Then, scalar surrogate models can be trained to predict the variations in each component of the vector $\boldsymbol{z_i}$. This procedure is called POD+Interpolation, one instance of which is the POD-PCE method where a PCE model is used in the latent space.

### B. Polynomial Chaos Expansion

Polynomial Chaos Expansion is a surrogate modeling technique that excels at uncertainty quantification and provides a rigorous mathematical framework based on probability theory. The central idea in PCE is to decompose a random variable into its deterministic and stochastic contributions using a linear combination of orthogonal polynomials [37–39].

To begin,let $\mathcal{M}$ represent a deterministic model which acts on a set of inputs and yields some vector output. Let $\boldsymbol{y}$ be the output in which each spatial location is a scalar random variable and let $\boldsymbol{\xi}$ represent a vector of random variables that determines the output. Thus, $\boldsymbol{y} = \{y_1, \ldots, y_n\}$ and is an element of $\boldsymbol{y} \in \mathbb{R}^n$, a vector that can represent the pressure or velocity field from a CFD simulation. Each component has some location, $\boldsymbol{x_i}$, in a 2D ($\mathbb{R}^2$) or 3D ($\mathbb{R}^3$) spatial domain, $\mathcal{D}_x$. And, $\boldsymbol{\xi} = \{\xi_1, \ldots, \xi_b\}$ is a b-dimensional vector where each component, $\xi_i$, is an independent random variable. The model maps the b-dimensional vector to another n-dimensional vector, i.e. $\mathcal{M} : \boldsymbol{\xi} \mapsto \boldsymbol{y} \in \mathbb{R}^n$.

For each $\xi_i$, one selects a family of polynomials $\left\{\Psi_{\alpha_i}^{(i)}(\boldsymbol{\xi_i})\right\}_{\alpha_i \in \mathbb{N}}$ with a polynomial order, $\alpha_i$. Define the inner product:

$$\langle \phi_1, \phi_2 \rangle_i = \int \phi_1(x)\phi_2(x) f_{X_i}(x) dx \tag{5}$$

For each random variable, using the underlying probability density function (PDF), $\rho_{\xi_i}$, it is possible to derive an associated set of orthogonal polynomials, $\boldsymbol{\Psi(\xi_i)}$, that satisfy

$$\begin{aligned} \left\langle \psi_i, \psi_j \right\rangle &= \int \psi_i(\xi_i)\psi_j(\xi_i)\rho_{\xi_i}(\xi_i) d\xi_i \\ &= \delta_{ij} \left\langle \psi_i^2 \right\rangle \end{aligned} \tag{6}$$

where $\delta_{ij}$ is the Kronecker delta, which equals 0 if $i \neq j$. Xiu and Karniadakis [38] found the orthogonal polynomial basis for common PDF distributions. These are summarized in Table 3 and offer exponential convergence rates of error for statistical moments [9, 10]. By multiplying each polynomial basis for every input variable with every other polynomial basis, we obtain the following multivariate basis, which is orthogonal with respect to the joint probability distribution of all the inputs:

$$\psi_\alpha(\boldsymbol{\xi}) = \prod_{i=1}^{d} \psi_{\alpha_i}^{(i)}(\xi_i) \tag{7}$$

Using this multivariate polynomial basis, it is possible to express $\boldsymbol{y}(\boldsymbol{x}, \boldsymbol{\xi})$:

$$\boldsymbol{y}(\boldsymbol{x}, \boldsymbol{\xi}) \equiv \mathcal{M}(\boldsymbol{x}, \boldsymbol{\xi}) = \sum_{\alpha=0}^{\infty} a_\alpha(\boldsymbol{x})\psi_\alpha(\boldsymbol{\xi}) \tag{8}$$

where $a_\alpha$ deterministic coefficients that vary with $\boldsymbol{x}$. Note that the multi-index notation used above represents a

complicated expression succinctly. For example, using multi-index notation, we can write:

$$P = a_0 D_0 + \sum_{i_1=1}^{\infty} a_{i_1} D_1\left(\xi_{i_1}\right) + \sum_{i_1=1}^{\infty} \sum_{i_2=1}^{i_1} a_{i_1 i_2} D_2\left(\xi_{i_1}, \xi_{i_2}\right) + \ldots \tag{9}$$

equivalently as,

$$P = \sum_{j=0}^{\infty} \alpha_j \psi_j(\xi_j) \tag{10}$$

where there is a pairing between $\alpha_j$ and $a_{i_1 i_2 \ldots i_n}$ and $\psi_j$ and $D_n\left(\xi_{i_1}, \xi_{i_2}, \ldots, \xi_{i_n}\right)$. Typically, one truncates the PCE expansion to some finite order $P$:

$$\boldsymbol{y}(\boldsymbol{x}, \boldsymbol{\xi}) \approx \mathcal{M}(\boldsymbol{x}, \boldsymbol{\xi}) = \sum_{\alpha=0}^{P} a_\alpha(\boldsymbol{x}) \psi_\alpha(\boldsymbol{\xi}) \tag{11}$$

A common way to truncate the expansion is to set an upper bound on the total degree of the polynomial expansion to $p$ such that

$$|\boldsymbol{\alpha}| = \sum_{i=1}^{d} \alpha_i \leq p \tag{12}$$

Thus, the total number of terms in the expansion is given by $P + 1 = (d + p)!/(d!p!)$.

The orthogonality property of a PCE enables the evaluation of statistical moments of the output using just the expansion coefficients:

$$\mu(\boldsymbol{y}) = \mathbb{E}\left[\boldsymbol{y}(\boldsymbol{x}, \boldsymbol{\xi})\right] \approx \int \left( \sum_{\alpha} a_\alpha \psi_\alpha(\xi) \right) \rho(\xi) d\xi = a_0(x) \tag{13}$$

and

$$\sigma^2 = \sum_{\alpha=0}^{P} a_\alpha^2(x) \langle \psi_\alpha, \psi_\alpha \rangle \tag{14}$$

This attribute of PCE whereby one can obtain closed form expressions for statistical moments using simply the coefficients is extremely powerful. Not only does this enable rapid estimations of statistics, but also reduces the reliance on further sampling the surrogate model to obtain moments.

*1. Regression-based PCE*

The estimation of PCE coefficients in Equation 8 can be found using intrusive, Galerkin projections, quadratures, or regression. Quadratures may request samples at points in the domain where the simulation cannot converge to an answer (which can occur frequently with CFD simulations at high angles of attack or complex geometries with complicated flow patterns). Najm [40] provides an overview of the different coefficient determination processes and Poette [41] provides an empirical comparison of different methods. While each of these methods are powerful, regression-based PCE is a versatile, low-cost, and flexible method that can be used with black-box analysis tools. The regression method for computing the PCE coefficients starts by generating $N \geq P + 1$ samples of the random vector $\boldsymbol{\xi}$. These $N$ samples are input into the simulation tool to generate snapshots of the system at various parameter settings. For the sake of simplicity, assume that the output of the simulation is a scalar, though these concepts readily extend to vector fields where each component can be considered an individual random variable. The coefficients $a_\alpha$ can be found by solving the following over-determined linear system:

$$\begin{pmatrix} \psi_0(\xi_0) & \psi_1(\xi_0) & \cdots & \psi_P(\xi_0) \\ \psi_0(\xi_1) & \psi_1(\xi_1) & \cdots & \psi_P(\xi_1) \\ \vdots & \vdots & \ddots & \vdots \\ \psi_0(\xi_N) & \psi_1(\xi_N) & \cdots & \psi_P(\xi_N) \end{pmatrix} \begin{pmatrix} a_0 \\ a_1 \\ \vdots \\ a_P \end{pmatrix} = \begin{pmatrix} y(\xi_0) \\ y(\xi_1) \\ \vdots \\ y(\xi_N) \end{pmatrix} \tag{15}$$

The least-squares problem above can be solved with a minimum of $P + 1$ samples, at which point the problem becomes one of solving a linear system of equations. However, in [17, 42], the authors found that an oversampling of at least

twice more than the required points yields a better approximation for the statistical moments. Not unexpected, as the number of training samples are increased, the greater the accuracy of the coefficients. The actual sampling method can be a space-filling design of experiments (DOE) or quasi-random Sobol sequence or latin hypercube sampling (LHS) DOE; however, results have shown that LHS and quasi-random Sobol sequence provide consistent performance in a variety of problems [17]. While the regression problem above is formulated using a traditional $L_2$-norm, one can easily modify the procedure to utilize an $L_1$-norm, which leads to a sparse regression. For further details on sparse PCE, the reader to referred to [14].

After the latent space coordinates of an unseen input parameter, $\boldsymbol{\xi}^*$, are estimated, the high-dimensional field is found through a process called *back-mapping*. For POD, back-mapping is carried out analytically by the projection $\mathbf{x}(\boldsymbol{\xi}^*) = \boldsymbol{\Phi}\mathbf{z}(\boldsymbol{\xi}^*)$.

## III. Methodology

The current section describes the POD-PCE method, which is a parametric, regression-based ROM that allows the user to predict uncertain fields. In general, the process of creating any ROM is divided into two steps: the offline step where the model is constructed and the online step where the model is evaluated for unseen parameters (see Figure 1). In the offline phase, the main steps are:

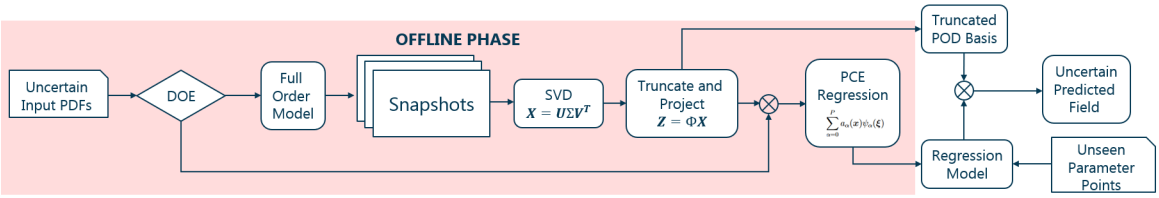


**Fig. 1 Flowchart of POD-PCE Method.**

1) *Identify design space*: Identify a set of $b$ uncertain parameters and their associated underlying PDFs, $\boldsymbol{\xi} = \{\xi_1, \ldots, \xi_b\} \in \mathbb{R}^b$.
2) *Generate high-fidelity data*: Sample $m$ combinations of design variables, $[\boldsymbol{\xi}_1, ..., \boldsymbol{\xi}_m] \in \mathbb{R}^{b\times m}$, using a DOE and evaluate the high-fidelity model to generate the solutions $\boldsymbol{X} = [\boldsymbol{x}_1, ..., \boldsymbol{x}_m] \in \mathbb{R}^{n\times m}$.
3) *Perform dimensionality reduction*: Perform POD to project $\boldsymbol{X}$ into a latent space $\boldsymbol{Z} = [\boldsymbol{z_1}, ..., \boldsymbol{z_m}] \in \mathbb{R}^{d\times m}$. $d$ is computed based on the desired $RIC$ threshold, $\delta$, such that $RIC(d) \geq \delta$.
4) *Generate PCE basis*: Based on each of the uncertain inputs, generate a multivariate polynomial basis, $\boldsymbol{\Psi_\alpha(\xi)}$, using the Askey scheme.
5) *Generate regression/interpolation model*: For each latent space coordinate, $z_i$, train a sparse PCE model using the regression procedure to obtain $\boldsymbol{g}$ such that $g_i : \boldsymbol{\xi} \mapsto z_i$.

In the online phase, the process is as follows:

6) *Predict latent variable*: For a given test point, $\boldsymbol{\xi}^*$, evaluate the PCE models, $\boldsymbol{g}$, to predict the latent coordinates, $\boldsymbol{z}^*$.
7) *Predict high-fidelity reconstruction*: Use the POD modes to perform the back-mapping procedure and produce a high-dimensional reconstructed solution.

Note that the above procedure is used for point predictions of the uncertain high-dimensional field. To calculate the mean and standard deviation, one can perform a Monte Carlo sampling of the ROM. This procedure would yield a precise estimate for the surrogate-predicted statistical moments, but one can also alternatively use the PCE coefficients to predict the moments. In particular, using the PCE models for each latent space coordinate, one can get analytical solutions for the latent space statistical moments, which can be subsequently propagated to the full-dimensional space using the POD modes.

### A. Error Metrics

The predictive accuracy of the above uncertain ROM is evaluated using multiple quantitative metrics across a set of validation cases. The first error metric characterizes the predictive performance of the ROM in estimating the mean and variance of the field. In the absence of exact expressions for the statistical moments, Monte Carlo analysis of the

full-order model represents the benchmark for estimating the mean and variance. The following componentwise relative error calculation can be used to visualize the error throughout the computational domain:

$$e = \frac{\hat{\boldsymbol{\mu}} - \boldsymbol{\mu}^*}{\max(\boldsymbol{\mu}^*)} \tag{16}$$

where $\boldsymbol{\mu}^*$ and $\hat{\boldsymbol{\mu}}$ are the exact mean and the predicted mean. The following integrated (scalar) measure of error using the $L_2$-norm can alternatively be used when comparing one ROM to another:

$$\mathrm{e} = \frac{\|\hat{\boldsymbol{\mu}} - \boldsymbol{\mu}^*\|_2}{\|\boldsymbol{\mu}^*\|_2} \tag{17}$$

One can readily use the above scalar and field-level error metrics for all statistical moments and point predictions.

The next error metric will be used to assess the accuracy of the ROM for every sample in the validation set. In particular, the following root mean square error (RMSE) calculation will be used:

$$\mathrm{e}_{\mathrm{RMSE,i}} = \sqrt{\frac{\sum_{j=1}^{N_t} (x^*_{j,i} - \hat{x}_{j,i})^2}{N_t}} \tag{18}$$

where $e_{\mathrm{RMSE,\,i}}$ is the error evaluated at the $i^{\mathrm{th}}$ node of the computational domain and $x_{j,i}$ is the solution at the $i^{\mathrm{th}}$ node of the vector $\boldsymbol{x}_j$. This will enable the user to qualitatively assess where a specific ROM deteriorates in accuracy. The normalized root mean square error (NRMSE) will be used as a scalar metric to assess the accuracy across multiple ROMs:

$$\mathrm{NRMSE} = \sqrt{\frac{\sum_{j=1}^{N_\mathrm{t}} \left\| \boldsymbol{x}^*_j - \hat{\boldsymbol{x}}_j \right\|^2}{\sum_{j=1}^{N_\mathrm{t}} \left\| \boldsymbol{x}^*_j - \overline{\boldsymbol{x}} \right\|^2}} \tag{19}$$

NRMSE can be further decomposed into a reconstruction and regression error. The reconstruction error is associated with how well the latent space models the physical space. More specifically, the reconstruction error represents the accuracy of the POD modes. The error is given by

$$\mathrm{e}_{\mathrm{rc}} = \sqrt{\frac{\sum_{j=1}^{N_\mathrm{t}} \left\| \boldsymbol{x}^*_j - \boldsymbol{\Phi}\boldsymbol{\Phi}^T \boldsymbol{x}^* \right\|^2}{\sum_{j=1}^{N_\mathrm{t}} \left\| \boldsymbol{x}^*_j - \overline{\boldsymbol{x}} \right\|^2}} \tag{20}$$

The regression error represents the accuracy of the interpolation models in capturing the latent space. This is given by

$$\mathrm{e}_{\mathrm{rg}} = \sqrt{\frac{\sum_{j=1}^{N_\mathrm{t}} \left\| \boldsymbol{\Phi}(\boldsymbol{\Phi}^T \boldsymbol{x}^*_j - \tilde{\boldsymbol{z}}) \right\|^2}{\sum_{j=1}^{N_\mathrm{t}} \left\| \boldsymbol{x}^*_j - \overline{\boldsymbol{x}} \right\|^2}} \tag{21}$$

## IV. Experimentation and Results

The methodology proposed in this study is evaluated on three test cases with varying numbers of inputs, outputs, shocks, and complexity. The test cases include uncertain flow through a converging-diverging nozzle, a function resembling supersonic flow over a 2D wedge with geometric uncertainties, and uncertain transonic flow over an RAE2822 airfoil.

### A. Converging-Diverging Nozzle

The aim of the first experiment is to work with a simple test function, also referred to as a canonical problem, that has the complexity of a high-fidelity simulation, but without the associated costs. The following test case analyzes steady flow through a converging-diverging nozzle with geometric uncertainties and is governed by:

$$\begin{aligned} \frac{\partial(\rho u A)}{\partial x} &= 0 \\ \frac{\partial(\rho u^2 A + \frac{pA}{\gamma})}{\partial x} - p\gamma\frac{\partial A}{\partial x} &= 0 \end{aligned} \tag{22}$$

where $A = A(x)$ is the area distribution, $\rho$ is density, $p$ is pressure, $u$ is velocity, and $\gamma$ is the specific heat ratio of the fluid. By specifying the boundary conditions at the entrance and exit, length of the nozzle, $L$, and the area distribution, one can iteratively solve for the Mach number, pressure, and density inside the nozzle. In this study, the exit area to throat area ratio ($A_e/A_t$) is uncertain and the pressure ratio throughout the nozzle is predicted. The area profile of the nozzle parabolically changes from $A(-L/2) = A(L/2) = 3$, with the throat located at $x = 0$. The length is set to 10 units. The boundary conditions, $p(-L/2) = 1$ and $p(L/2) = 0.7$, are chosen such that the shock forms in the diverging portion of the nozzle.

The throat area is a uniform random variable on [0.75, 1]. The solution is obtained by discretizing the governing equations over a uniform grid of 1000 points over space and using a second-order central finite difference scheme. A LHS sampling DOE is used to generate $m$ samples for training and $N_t = 10,000$ for validation. The number of training samples is varied ($m = [25, 50, 100, 200, 300]$) to see the impact of sparse data sets on the predicted outcome.

Figure 2 shows the predicted response for a specific test case for both a low order and high order PCE regression. It is seen that the POD-PCE model is able to accurately predict the response in the regions away from the shockwave; near the shockwave, there is significant error. This behavior is referred to as the Gibbs' phenomenon and is characterized by the following traits:

- Near discontinuous features, the solution exhibits overshoots and undershoots
- For low order PCE models, the oscillations can last for large distances and have high magnitudes
- With increasing PCE order, the oscillations reach higher frequencies

This indicates that approximating a nonlinear space with a linear subspace naturally leads to errors, irrespective of the latent space regression model used.

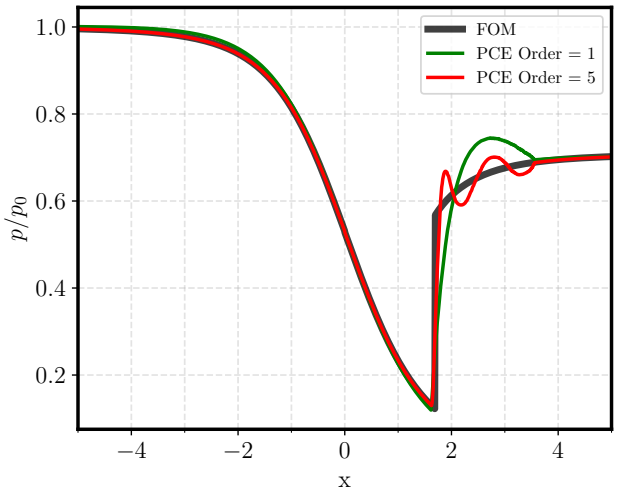


**Fig. 2 Pressure variation inside a converging diverging nozzle for $A_e/A_t = 7.38$. Note that the ROM is trained using 300 samples.**

Figure 3 provides a visualization of the RMSE at each node in the computational domain for a ROM built using 300 samples and two different PCE regressions. The 1$^{st}$ order model has a large error throughout the computational domain, though the RMSE is ten times higher near the shockwave due to the Gibbs' phenomenon. As order increases, the latent space regression improves and the reconstructed solution is more accurate. This diminishes the error in the regions away from the shock, but the solution continues to exhibit oscillations near the discontinuity. Figure 3b provides a more refined assessment of error as the PCE order increases. It is seen that as order increases, error monotonically decreases. This is because flows with shockwaves have a slow eigenvalue decay and thus a large number of POD modes are required to meet the $RIC = 0.9999$ threshold. However, these POD modes have highly nonlinear variations which increase the complexity of the latent space and necessitate the use of higher order PCE models. In fact, though the error is decreasing, there is no clear asymptote, which indicates that even a 5$^{th}$ order expansion is insufficient to accurately model the latent space. As samples increase, the error decreases, although more marginally than with changes in order. This is because additional samples added to the training set only offer minute improvements to the POD modes.

Figure 4 shows the variations in the reconstruction and regression error that contribute to NRMSE as the order and samples are varied. The reconstruction error is not impacted by the PCE order as it purely depends on the dimensionality

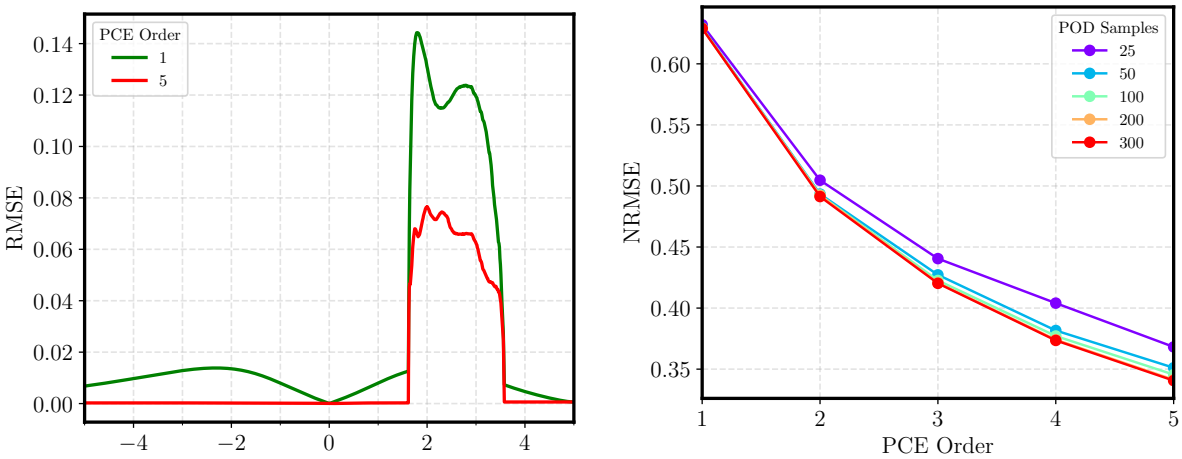


**(a) RMSE variation for model trained using 300 samples.** **(b) NRMSE variation with order and training samples.**

**Fig. 3 Impact of training sample size and PCE order on error.**

reduction procedure. The diminishing returns offered by the addition of training data is clear: The error decreases by approximately 30% as the training data is increased from 25 to 50. But, the error only changes by 12% when the samples increased from 200 to 300. Note that the number of POD modes required to capture the RIC increases rapidly with training samples (see Table 4). Thus, for a fixed PCE order, the regression error increases with sampling data as the latent space has more nonlinearity and larger dimensionality. In fact, the regression error contributes to over 75% of the NRMSE and sometimes close to 90%, indicating the difficulty of modeling the POD latent space. Figure 5 shows

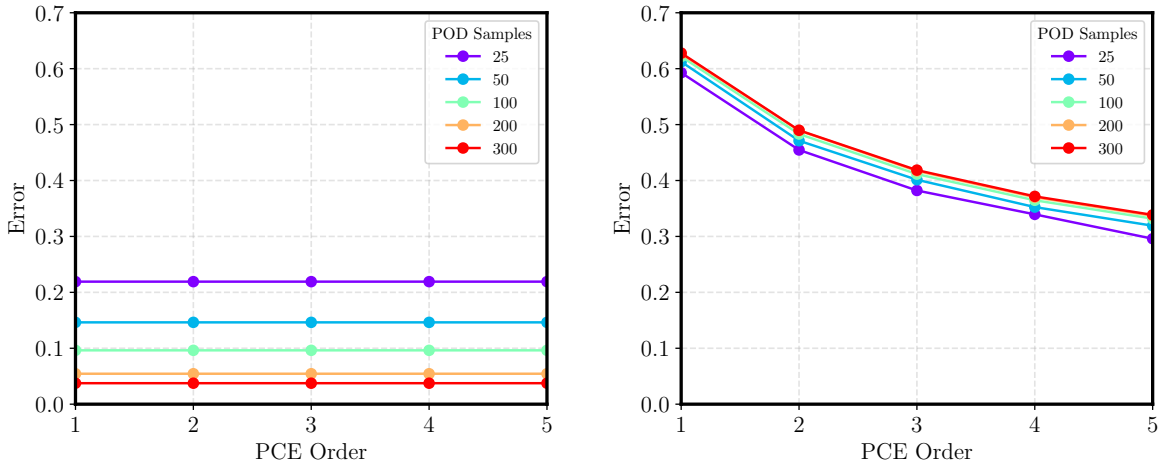


**(a) Reconstruction Error** **(b) Regression Error**

**Fig. 4 Impact of training sample size and PCE order on the reconstruction and regression errors.**

the statistical moments calculated using a Monte Carlo analysis of the full-order and surrogate model and analytical formulas using the PCE coefficients. The mean response shows a gradual variation in pressure caused by averaging the shockwave across multiple samples. The variance response has the highest magnitude between $x = [1.5, 3.6]$ as the shockwave is varying most in this interval. The analytically calculated mean for a sparse PCE model is different from the MC results both near and away from the shockwave. On the other hand, the mean calculated using MC of the surrogate is indistinguishable from the exact MC response for both low order and high order PCE expansions. The fundamental reason the analytical response has a much larger error compared to MC of the surrogate is due to the use of sparse regression. Specifically, as the mean response depends only on the first PCE coefficient, and, in case of a sparse

**Table 4 CD Nozzle - POD modes retained to capture 99.99% variance.**

| Samples | Modes Retained |
|---|---|
| 25 | 4 |
| 50 | 49 |
| 100 | 88 |
| 200 | 137 |
| 300 | 159 |



regression, many terms from the full PCE are dropped, there is a loss of information and the PCE coefficients change. This leads to inaccuracies in the analytical formulas. However, if the $L_2$-norm is used during regression, the mean response obtained analytically is equally as accurate as that obtained using MC (see Figure 5a).

The variance predicted using the different approaches is not vastly different, though each model has a marked error compared to the exact variance. This is because the variance computation depends on the square of all PCE coefficients and those coefficients that were dropped during sparse regression had small magnitudes. While an increase in order does improve the accuracy of the predicted variance, the $5^{\text{th}}$ order PCE model is still unable to predict the maximum variance. The error for variance is driven primarily by the RIC used during dimension reduction and is discussed in more detail later. Though these figures show the powerful theoretical properties of PCE methods that help circumvent the use of MC and rapidly predict the statistical moments, full PCE models are computationally expensive to train and difficult to interpret due to the large number of terms. Thus, for the remaining experiments, all statistical moments are calculated using MC and sparse PCE as they provide accurate estimates and enable the development of parsimonious models.

Figure 6 presents the impact of varying training samples and PCE order on the relative $L_2$-norm error for the mean and variance. In both plots, the addition of samples offers diminishing returns to reducing the error. The POD-PCE method is able to accurately predict the mean response with the error unaffected by order. To reduce the error for variance, one must simultaneously use high order PCE models and retain many POD modes to ensure that the inaccuracy introduced during dimensionality reduction and regression is minimized.

### B. Supersonic Flow over Oblique Wedge

The following problem is a two-dimensional analytical step function meant to resemble supersonic flow over a wedge with an attached oblique shock. This function closely matches the stochastic simulations performed with wedges in supersonic flow by several authors [17, 43]. The analytical function enables the direct control of features of interest without a significant simulation cost. The three uncertain parameters in this problem have different PDFs and thus introduce an increased level of complexity during modeling. The spatial domain is discretized using a $100 \times 100$ grid and the field response that is predicted in this test problem is given by the following governing equation:

$$f(x, y; a, \beta, \delta) = \begin{cases} a^2 + 10, & \text{if } y \leq x \tan(\beta + \delta) \\ 10, & y > x \tan(\beta + \delta) \end{cases} \tag{23}$$

where $a$ determines the shock step size, $\delta$ is the wedge angle, and $\beta$ is the shock angle relative to the wedge surface. The wedge and shock angles are described by a Gaussian distribution with a mean value of $10^\circ$ and standard deviation of $2^\circ$. The parameter $a$ represents in-flow uncertainty and is distributed uniformly in $[8, 11]$.

Figure 7 shows the predicted response for one set of unseen parameters using the POD-PCE method. Similar to the behavior seen in the previous experiment, POD is able to predict the response in linear regions (away from shocks) with high accuracy and has the largest magnitude of error localized near nonlinear structures (near the shock). Because the shockwave is reconstructed as a "staircase" pattern, the highest error occurs at the true location of the shockwave and persists away from the shockwave. The componentwise RMSE in Figure 8 provides a visualization of the global error variation over all samples in the validation set. In both plots, it is clear that as we move farther away from the discontinuity, the accuracy of the ROM improves. Further, as the PCE order is increased, the magnitude of the maximum RMSE decreases by 24% from 24.9 to 18.9, though the region of error remains the same. This indicates that though the latent space is being more accurately predicted, the limitations of a linear reconstruction procedure remain (i.e. Gibbs'

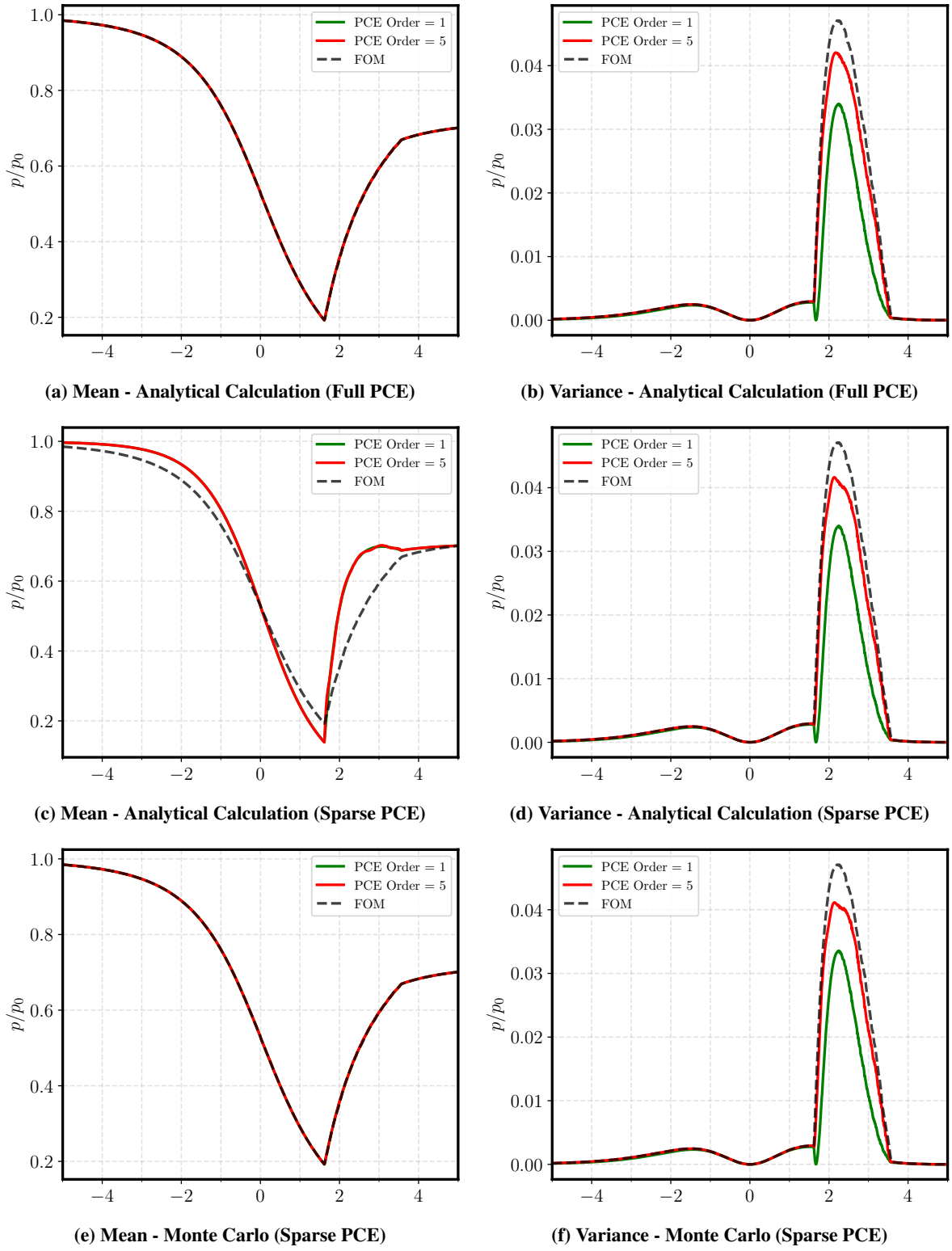


(a) Mean - Analytical Calculation (Full PCE)

(b) Variance - Analytical Calculation (Full PCE)

(c) Mean - Analytical Calculation (Sparse PCE)

(d) Variance - Analytical Calculation (Sparse PCE)

(e) Mean - Monte Carlo (Sparse PCE)

(f) Variance - Monte Carlo (Sparse PCE)

**Fig. 5 Exact vs. predicted statistical moments due to uncertainty in geometry inside a CD nozzle.**

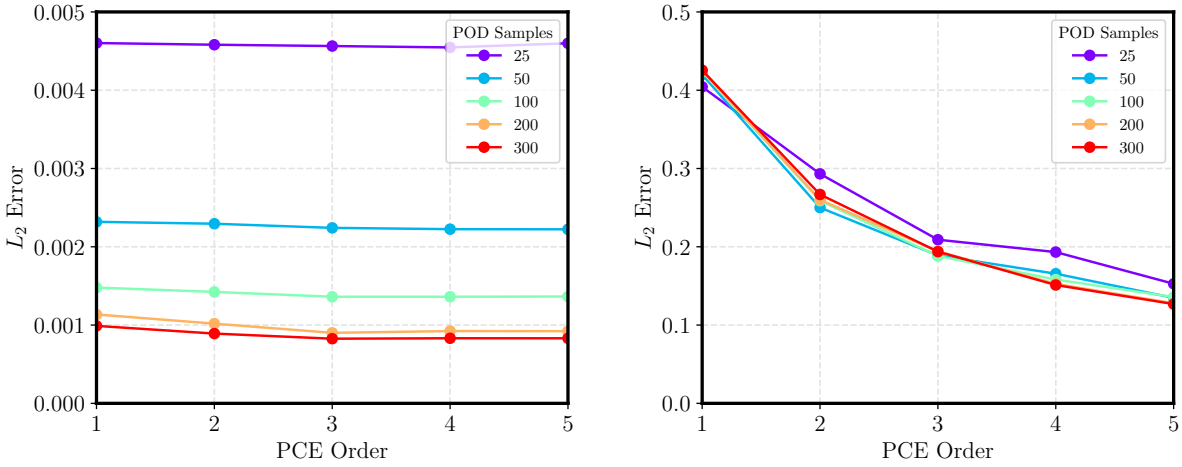


**(a) Mean** **(b) Variance**

**Fig. 6 Impact of training sample size and PCE order on the integrated errors for statistical moments.**

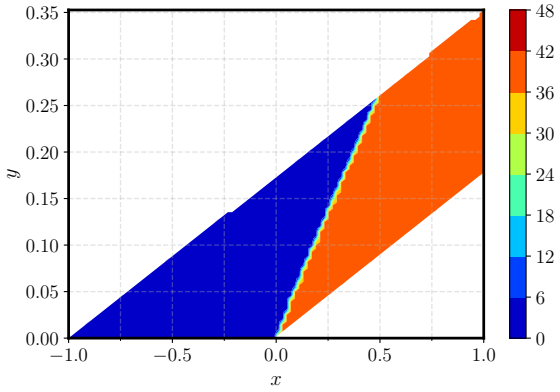


**(a) FOM**

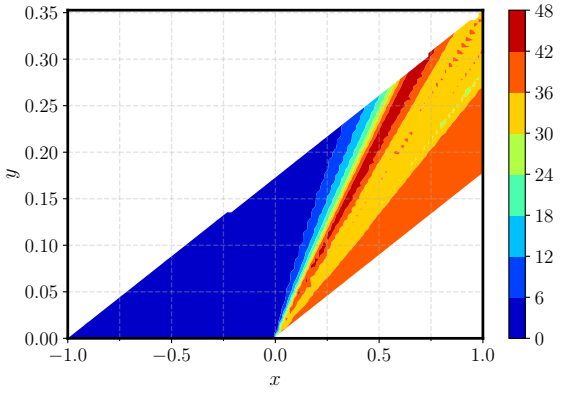


**(b) POD-PCE trained using 400 samples and a 5$^{th}$ order PCE**

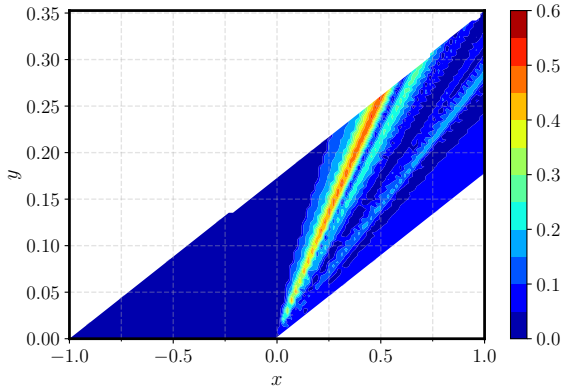


**(c) Componentwise relative error**

**Fig. 7 Comparison of the FOM solution to the predicted solution found using POD-PCE for one set of uncertain inputs.**

phenomenon) and the neighborhood around the nonlinear shock has a degradation in accuracy. Thus, the POD-PCE method is most proficient in problems where the shockwave occupies a small portion of the entire computational domain.

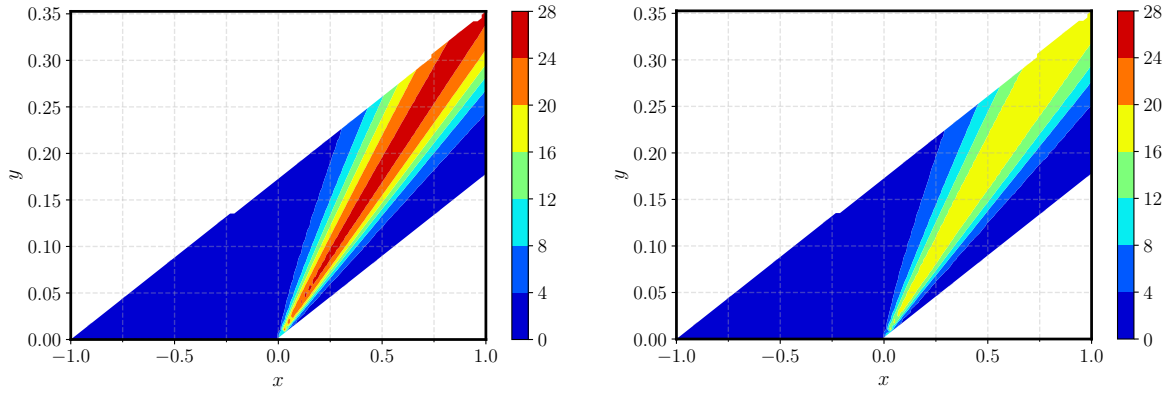


**(a) (Samples, Order) = (400, 1st)** **(b) (Samples, Order) = (400, 5th)**

**Fig. 8 Impact of training sample size and PCE order on the RMSE for different PCE orders.**

Figure 9a provides a detailed performance overview of the POD-PCE method using NRMSE. The NRMSE closely resembles the regression error, indicating that the accurate prediction of the latent space dictates the performance of the ROM. By increasing the number of the training data points, NRMSE consistently decreases but with diminishing returns. In fact, the differences ROMs are near indistinguishable when low order PCE models are used because there are few coefficients to fit and capture nonlinearities. For data sets with 50 samples, the NRMSE decreases only until a 2nd order expansion. After this point, the number of samples supplied to PCE is insufficient and falls below the recommended 2x oversampling ratio to fit the coefficients of the PCE model. This causes an increase in the regression error, the NRMSE for the training data set, and NRMSE for the validation data set. As the number of samples is increased, there is sufficient information to train higher order PCE models, but over-fitting becomes prevalent. For example, ROMs trained using 100 and 200 samples and a 4th order expansion can fit the training data well (seen through a reduction in training NRMSE), but the results in the validation set show a rise in error. This is a characteristic performance seen in over-fit PCE models. For samples $\geq 300$, the error consistently decreases with PCE order as there is sufficient data to fit the coefficients.

Thus, to improve the performance of POD-PCE models in flows with shockwaves, it is important to simultaneously increase the number of training samples and the PCE order; however, the practitioner should monitor the results for over-fitting. Lastly, as seen through Table 5, the POD procedure requires a significant number of modes to capture the nonlinearity. These higher-order modes introduce highly nonlinear variations in the latent space that are challenging to model and decrease model parsimony; thus, alternative methods for dimensionality reduction procedure should also be investigated.

**Table 5 2D Wedge - POD modes retained to capture 99.99% variance.**

| Samples | Modes Retained |
|---|---|
| 50 | 45 |
| 100 | 90 |
| 200 | 177 |
| 300 | 257 |
| 400 | 332 |

Figure 10 presents the statistical moments calculated using a Monte Carlo analysis of the full-order model and those obtained using the surrogate model. The mean response shows the shockwave spread across multiple cells and is captured precisely with the POD-PCE method, with a near-zero relative error. Further, it is seen that the region of error

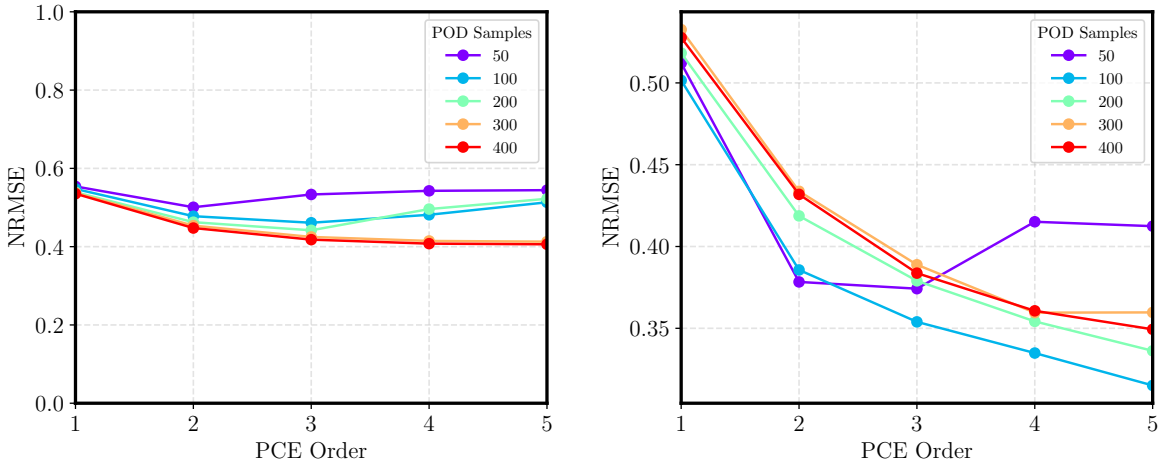


**(a) NRMSE over validation set**




**(b) NRMSE over training set**

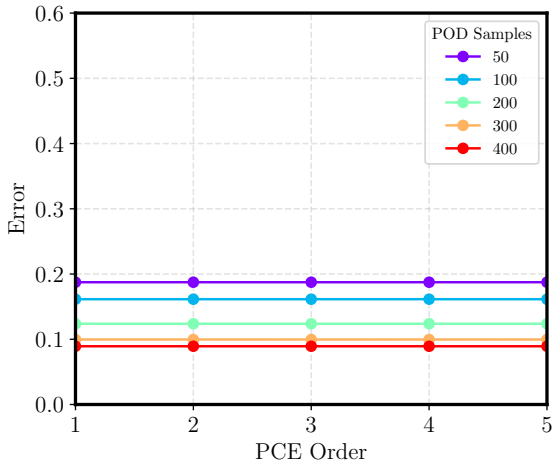


**(c) Reconstruction error**

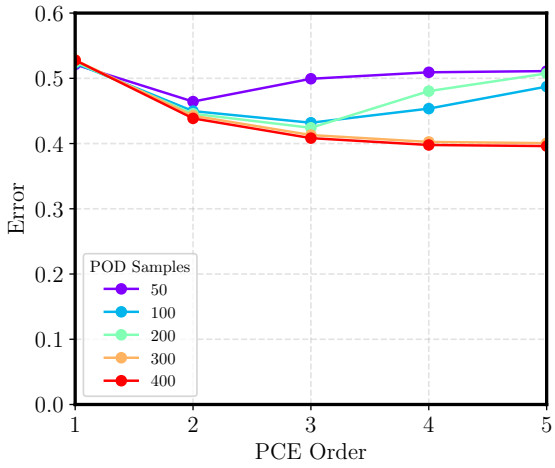


**(d) Regression error**

**Fig. 9 Impact of training sample size and PCE order on the NRMSE, reconstruction error, and regression error.**

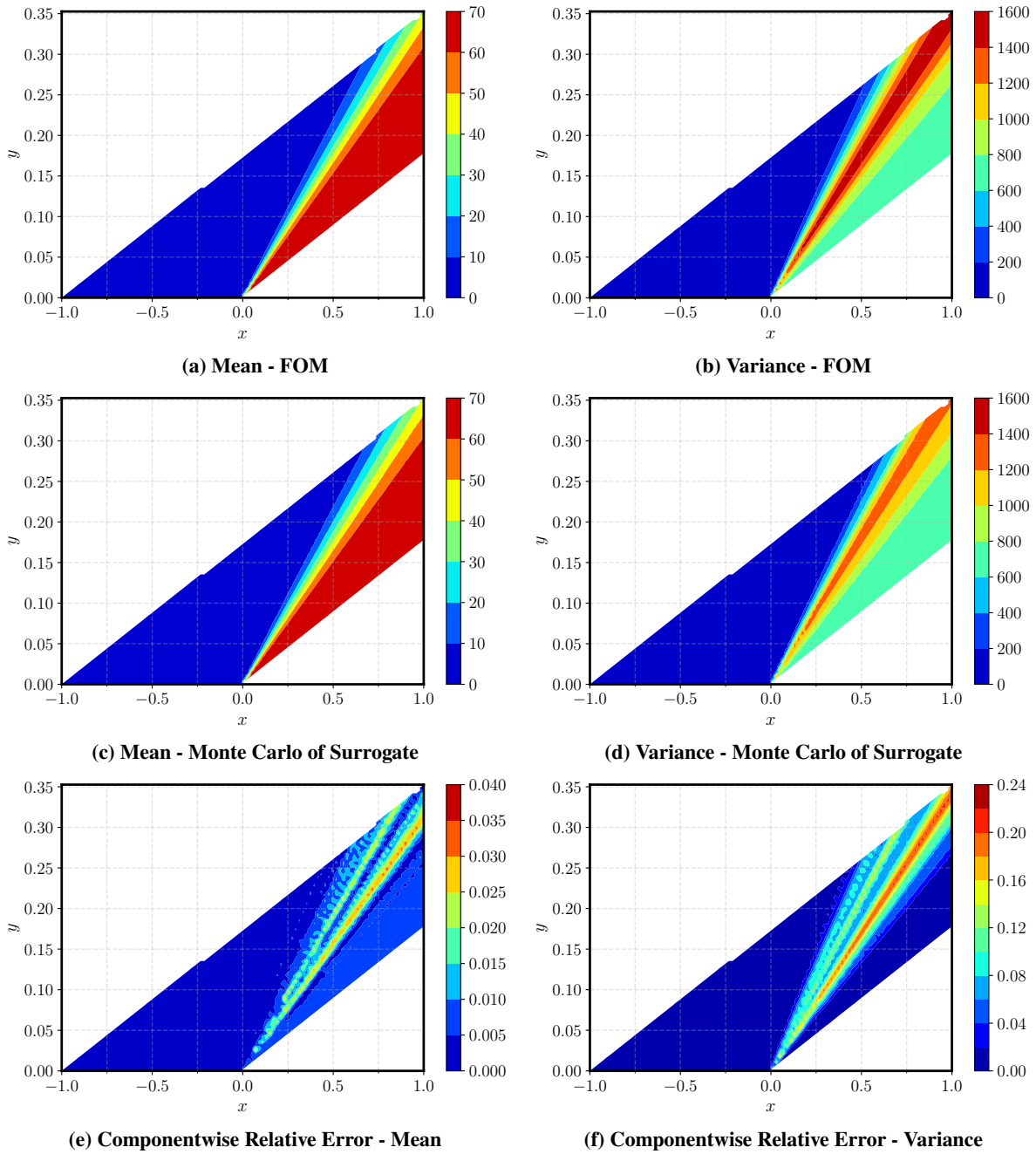


**(a) Mean - FOM**

**(b) Variance - FOM**

**(c) Mean - Monte Carlo of Surrogate**

**(d) Variance - Monte Carlo of Surrogate**

**(e) Componentwise Relative Error - Mean**

**(f) Componentwise Relative Error - Variance**

**Fig. 10 Exact vs. predicted statistical moments for 2D Wedge. Note that the ROMs were trained using 400 samples and a $5^{th}$ order PCE.**

for the mean and variance is approximately the same. Specifically, the error region is small near the nose of the cone, but increases in size as we move away from the apex. This is because the variability of the shock increases and the linear POD modes fail to capture the larger nonlinear variations. Thus, POD-PCE method has superior performance in flows with smaller variance from shockwaves.

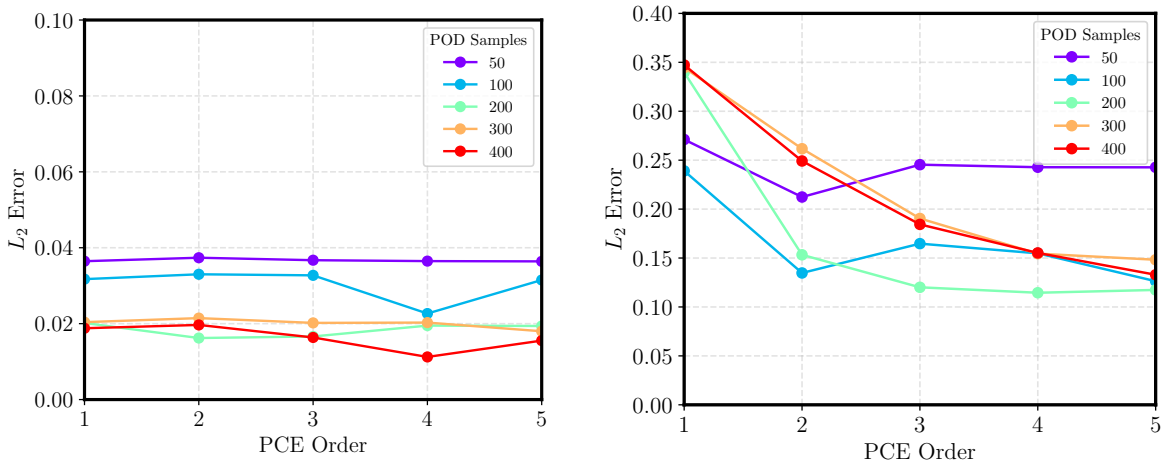


**(a) Mean** **(b) Variance**

**Fig. 11 Impact of training sample size and PCE order on the integrated errors for statistical moments.**

Figure 11 shows the impact of varying training samples and PCE order on the integrated error for statistical moments. For the mean, the order has no impact on the predictive accuracy, and increasing samples monotonically decreases error. On the other hand, the error for predicted variance clearly decreases with order and generally does not decrease with increasing samples. Lastly, note that the variance error is consistently an order of magnitude higher than that for the mean. These facts were seen in the previous test case and can be explained as follows: During dimensionality reduction, POD identifies a latent space where the principal vectors capture the most variance in the data. However, several modes, especially those associated with the higher frequency variations, are truncated as they do not add significant energy to meet the relative information content criteria. Thus, by selecting the RIC, one sets the maximum accuracy of the POD model for capturing the variance. To improve the accuracy of the variance response, it is important to not only increase the RIC, but also increase the PCE order to capture the nonlinearities introduced in the latent space through the higher frequency modes.

### C. RAE2822 Airfoil in Transonic Flow

The goal of this test case is to assess the ability of the proposed methodology in predicting the pressure field around an airfoil in transonic flow with geometric and angle of attack uncertainty. Geometric uncertainty is introduced by using a Free Form Deformation (FFD) approach (see Figure 12). In particular, the shape of an RAE2822 airfoil is varied by vertically displacing control points of a box that bounds the outer shape [44]. Here, only two control points at the mid-chord of the airfoil are used to perturb the shape. Note that control points at the edges are fixed to independently control angle of attack. Control point displacement is limited to $\pm 3\%$ of the chord length and is uniformly distributed in the interval $[-3\%, 3\%]$. The Mach number is fixed at 0.725 and angle of attack is represented by a uniform random variable over the interval $[-2°, 2°]$. In such flow conditions, a shock develops on the upper surface of the airfoil, which changes with input uncertainties.

The simulations are performed using the SU2 code and solve the RANS equations with a Spalart-Allmaras (SA) turbulence model over an O-grid domain (see Figure 13). The entire mesh has 10,500 nodes. A database of 1,000 samples is generated using an LHS DOE. Models are trained using randomly selected samples from this database to assess the accuracy of the ROM to different training set sizes. The number of training samples is varied, ($m = [50, 100, 200, 300, 400]$), with 1,500 points used for validation.

Figure 14 compares the exact CFD solution to that obtained using the ROM at one test point. Similar to the performance seen in the previous experiments, the POD-PCE method is able to accurately predict the pressure distribution

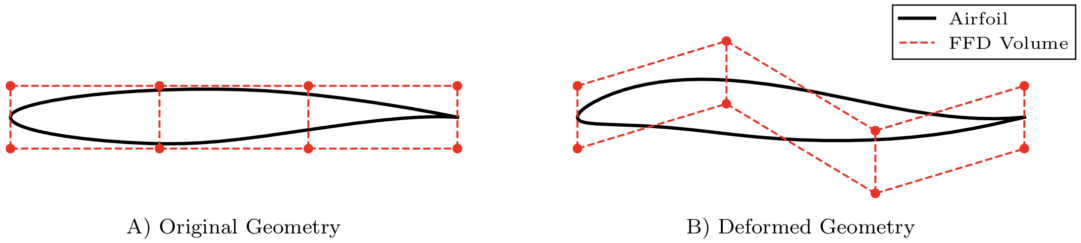


**Fig. 12 Notional shape perturbation using FFD**

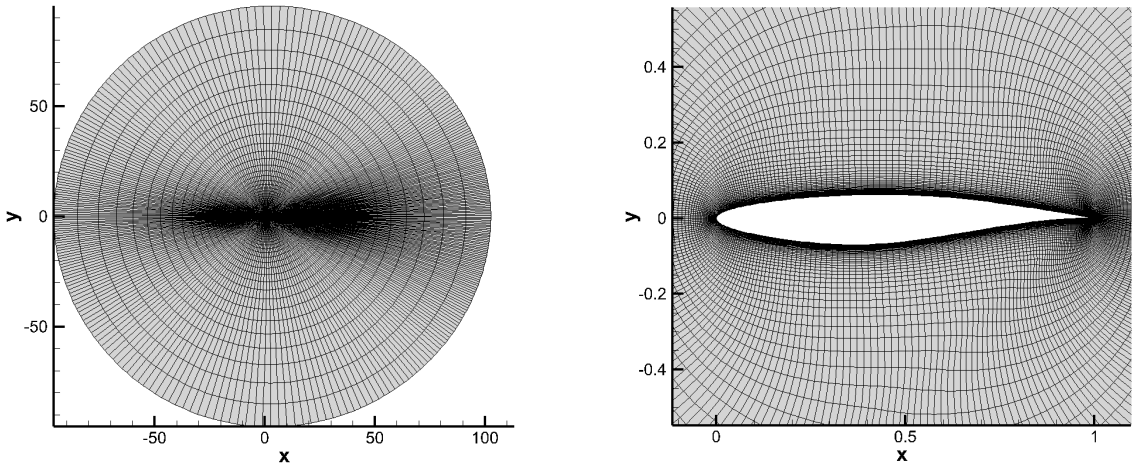


**Fig. 13 RAE2822 - CFD grid**

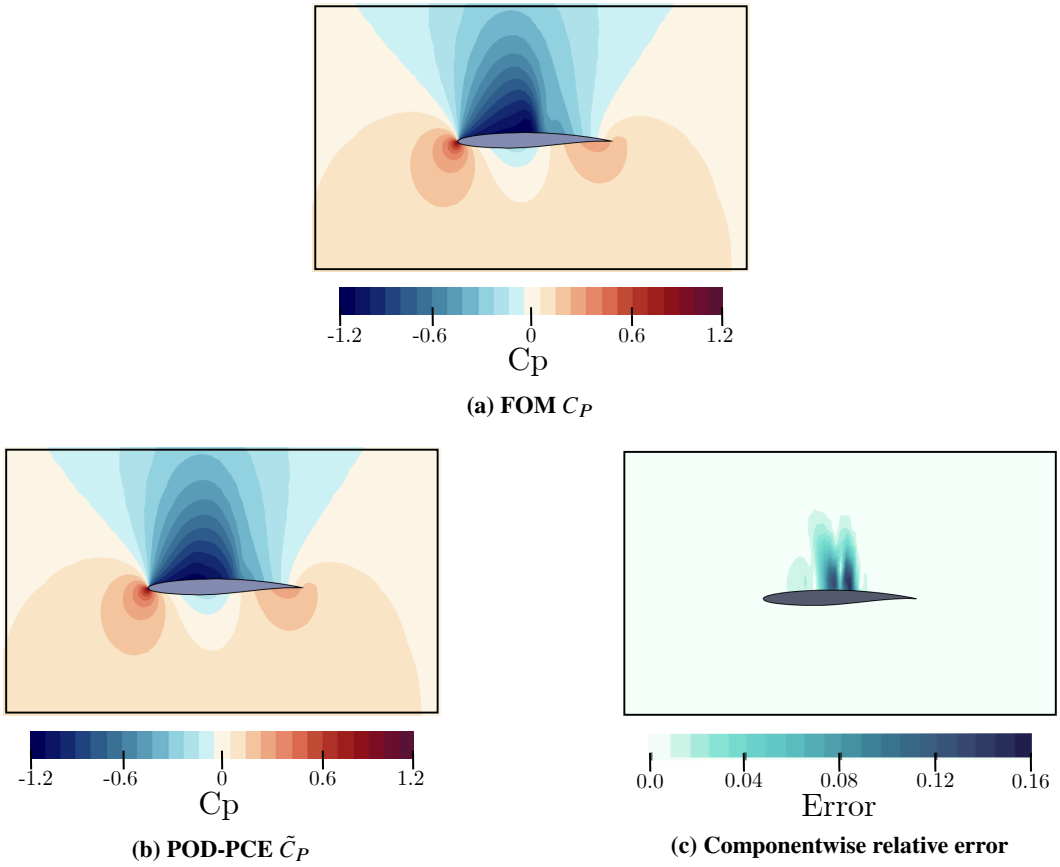


**(a) FOM $C_P$**

**(b) POD-PCE $\tilde{C}_P$**

**(c) Componentwise relative error**

**Fig. 14 RAE2822 - Flow visualization for the predicted $C_P$ and relative prediction error for POD-PCE. Solutions are for ROM trained with 400 samples and a 5$^{th}$ order expansion.**

around the airfoil when the flow is subsonic, and therefore devoid of shockwaves. However, the ROM inaccurately predicts the location of the shockwave, which leads to a large increase in error.

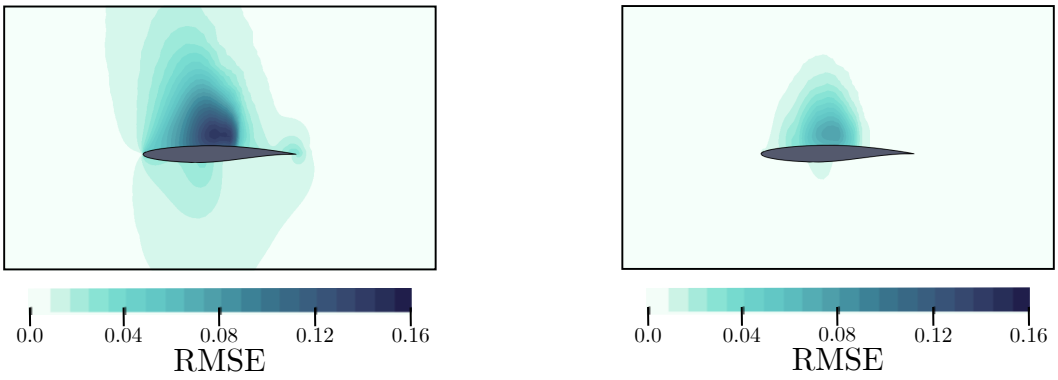


**(a) (Samples, Order) = (400, 1st)** **(b) (Samples, Order) = (400, 5th)**

**Fig. 15 RAE2822 - Visualization of RMSE**

Figure 15 shows the RMSE variation over the entire computational domain evaluated over the validation data set. The RMSE is largest in the region near the discontinuity and small near the leading edge and trailing edge, irrespective of the PCE order used. However, as the PCE order increases, the maximum RMSE value over the entire domain decreases by 47% from 0.144 to 0.0758. This performance improvement manifests as a 61% decrease in NRMSE. Figure 16a shows the variation of the NRMSE for different training samples and PCE orders. As the PCE order increases, there is a monotonic decrease in error except for the 50 sample case. This is because a $4^{th}$ order expansion requires at a minimum 35 samples, though it is recommended that 70 samples (2x oversampling ratio) be provided for the regression procedure. A $5^{th}$ order model requires at a minimum 56 samples. Though the paper uses a sparse regression procedure, as the PCE order increases, the oversampling ratio decreases as more terms are added and leads to a decrease in accuracy. This behavior is seen in both the 50 and 100 sample case for high PCE orders, but is not evident for larger training data sets. Thus, for fixed PCE order, as samples increase, we see a monotonic decrease in error as the POD modes improve in accuracy and PCE models have higher oversampling ratios during regression. Note that unlike the previous test cases, the number of modes retained does not change after 200 training samples (see Table 6), which fixes the dimensionality of the latent space.

Figure 16 shows the reconstruction and regression error variation. The reconstruction error is an order of magnitude smaller than the regression error indicating the difficulty that the PCE model has in regressing the latent space. Reconstruction error decreases as the sample size grows, though the information gathered from the data becomes saturated beyond 300 samples. As the number of modes does not change after 200 samples, any change in the reconstruction error is due improvements in the accuracy of the modes. As the number of samples increases, there is a

**Table 6 RAE2822- POD modes retained to capture 99.99% variance.**

| Samples | Modes Retained |
|---|---|
| 50 | 17 |
| 100 | 19 |
| 200 | 21 |
| 300 | 21 |
| 400 | 21 |

decrease in regression error for a fixed PCE order. For ROMs trained with sparse data sets, there is a rapid asympotote in the regression error as the PCE order increases. The asymptote occurs at larger PCE orders and leads to smaller

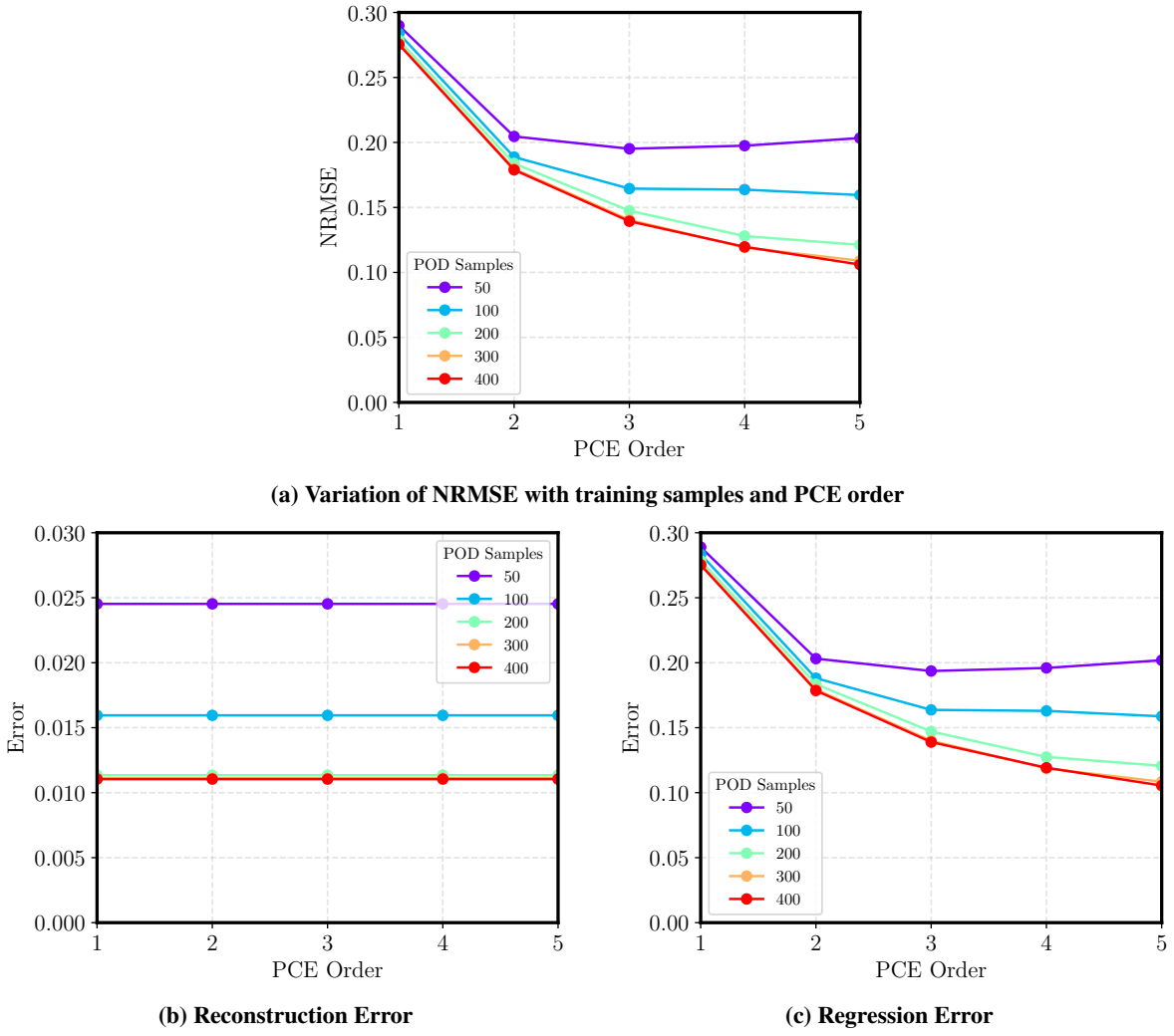


**(a) Variation of NRMSE with training samples and PCE order**

**(b) Reconstruction Error**

**(c) Regression Error**

**Fig. 16 Impact of training sample size and PCE order on the NRMSE, reconstruction error, and regression error.**

overall errors when the sample size is large because of the increased information available through the training data and terms in the PCE model.

Figure 17 and 18 present the statistical moments calculated using a Monte Carlo analysis of the full-order model and those obtained using the surrogate model. Note that, as the geometry changes due to uncertainty, the plots presented are moments scaled back to the mesh for the mean airfoil shape and angle of attack. In both the mean and variance plots, the error is largest near the shockwave. The point of maximum variance occurs near the airfoil leading edge and not near the shockwave. However, the error is largely on the upper airfoil surface and reaches a maximum value near the shock. Predictive accuracy improves rapidly as we move away from the shockwave, where variations are smoother, though not necessarily smaller. This indicates that though the POD-PCE method performs well in predicting fields with large variance, there is sharp decrease in predictive accuracy due to shockwaves. As expected, if the order of the PCE model increases, the latent space is captured more accurately and the magnitude of error decreases.

Figure 19 show the impact of varying training samples and PCE order on the integrated error for the mean and variance. Overall, the mean response is predicted accurately, and performance improves marginally if PCE order increases and the uncertain PDFs are sampled more densely. On the other hand, the error for variance is an order of magnitude higher. As discussed previously, samples do not play a strong role in decreasing the error because the RIC dictates the amount of variance captured. In cases where the number of samples is large (enough to meet the oversampling ratio requirements for PCE), the error decreases with increasing PCE order (as seen in Figures 18c and 18e).

## V. Conclusion

Polynomial chaos expansions (PCE) and reduced order modeling (ROM) are two essential enablers for bringing high-fidelity simulation tools earlier in the design process and rapidly quantifying uncertainty. However, over the past two decades, as PCE and ROM have progressed in their individual disciplines, they combined usage has not been thoroughly explored. This study explores the use of PCE in combination with Proper Orthogonal Decomposition (POD) to propagate uncertainty in high-dimensional fields with highly nonlinear structures, such as shocks. The performance of the proposed non-intrusive, parametric, POD-PCE method is assessed using a series of canonical problems and CFD-based test cases. It is seen that POD-PCE method is able to accurately predict the response in the regions away from discontinuous features, such as shockwave; but, near shockwaves, there is significant degradation in predictive accuracy. This deficiency is due to approximating a nonlinear space with a linear combination of POD modes. Thus, the POD-PCE method is most proficient in problems where the shockwave occupies a small portion of the entire computational domain.

It is seen that as the PCE order increases, global predictive error monotonically decreases. The performance also improves as the number of training samples is increased, though with diminishing returns. In general, even with using sparse PCE methods, it is recommended that if the order is increased, the training samples also be increased to ensure sufficient information is provided for the latent space fitting procedure. Results show that the accurate prediction of the latent space dictates the performance of the ROM. The POD-PCE method accurately predicts the mean response with near-zero error in all test cases. The method also performs well in predicting fields with large variance, but there is sharp decrease in predictive accuracy due to shockwaves. To improve the accuracy of the variance response, it is recommended that the RIC used during POD and the PCE order be increased to ensure the higher frequency modes associated with shock movement are captured well. As such, alternative methods for dimensionality reduction procedure should be investigated when addressing problems with discontinuities, as POD leads to relatively complex latent spaces that are difficult to regress.

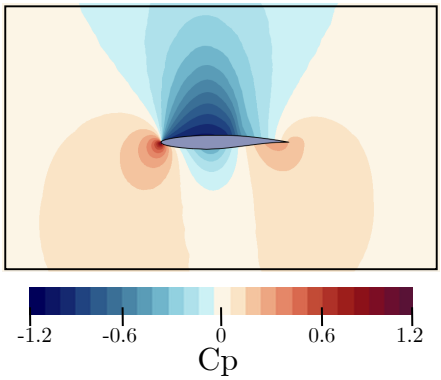


**(a) FOM - Mean $C_P$**

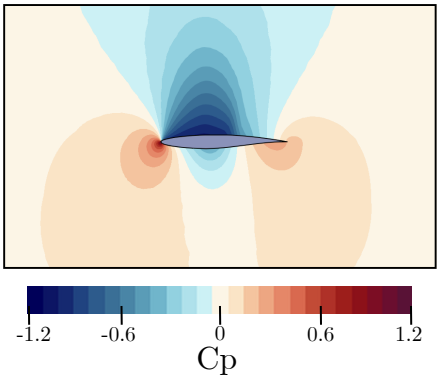


**(b) POD-PCE (1st Order PCE), Mean $\tilde{C}_P$**

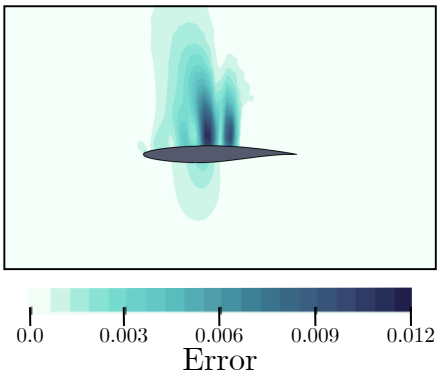


**(c) Componentwise Relative Error**

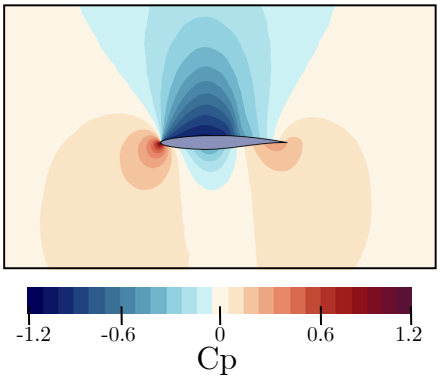


**(d) POD-PCE (5th Order PCE), Mean $\tilde{C}_P$**

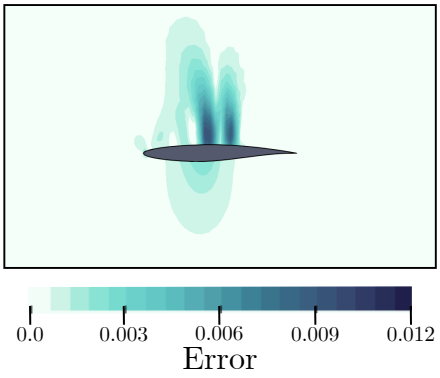


**(e) Componentwise Relative Error**

**Fig. 17 RAE2822 - Flow visualization for the predicted mean $C_P$ and relative prediction error for different PCE orders. Solutions are for ROM trained with 400 samples.**

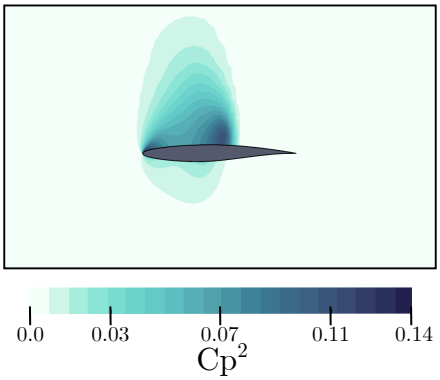


**(a) FOM, Variance $C_P$**

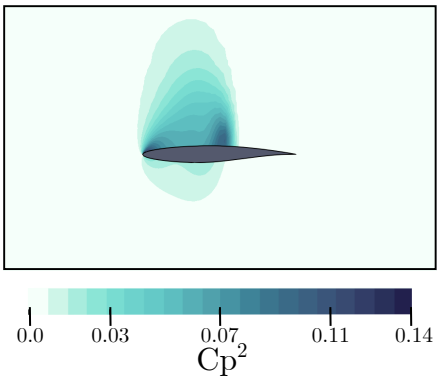


**(b) POD-PCE (1st Order PCE), Variance $\tilde{C}_P$**

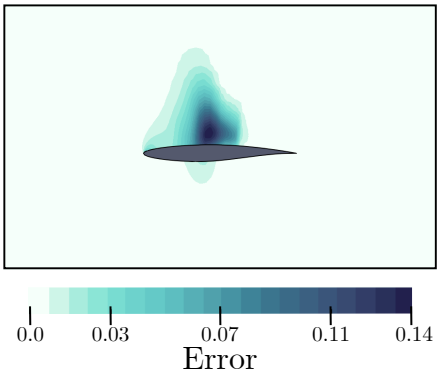


**(c) Componentwise Relative Error**

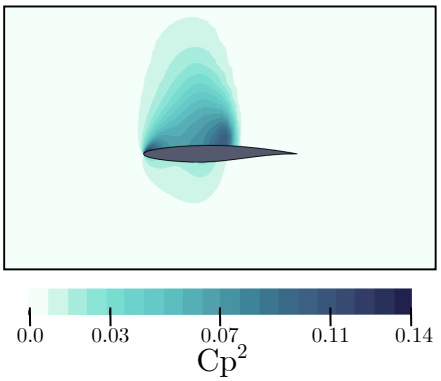


**(d) POD-PCE (5th Order PCE), Variance $\tilde{C}_P$**

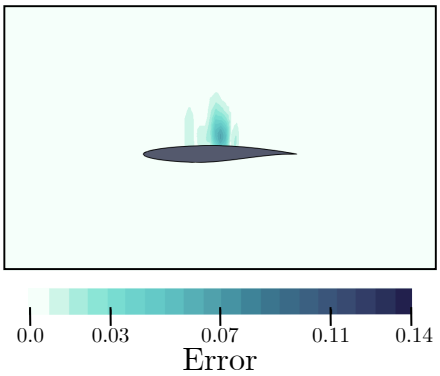


**(e) Componentwise Relative Error**

**Fig. 18 RAE2822 - Flow visualization for the predicted $C_P$ variance and relative prediction error for different PCE orders. Solutions are for ROM trained with 400 samples.**

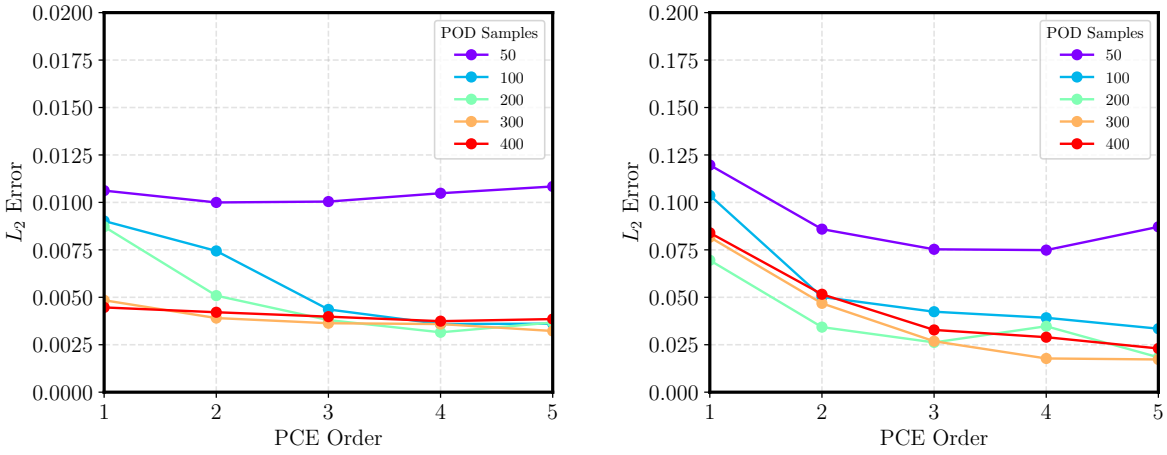


**(a) Mean** **(b) Variance**

**Fig. 19 RAE2822 Airfoil - Impact of training sample size and PCE order on the integrated errors for statistical moments.**

# References


[1] Slotnick, J. P., Khodadoust, A., Alonso, J., Darmofal, D., Gropp, W., Lurie, E., and Mavriplis, D. J., "CFD vision 2030 study: a path to revolutionary computational aerosciences," Tech. rep., 2014.

[2] Ishikawa, H., Ueno, A., Koganezawa, S., Makino, Y., Liebhardt, B., and Lütjens, K., "Sensitivity study and primary boom carpet assessment for conceptual low boom supersonic transport," *AIAA Scitech 2021 Forum*, , No. January, 2021, pp. 1–14. doi:10.2514/6.2021-0608.

[3] Ordaz, I., and Li, W., "Using CFD surface solutions to shape sonic boom signatures propagated from off-body pressure," 2013, pp. 1–10. doi:10.2514/6.2013-2660.

[4] Chatterjee, T., Chakraborty, S., and Chowdhury, R., "A Critical Review of Surrogate Assisted Robust Design Optimization," *Archives of Computational Methods in Engineering*, Vol. 26, No. 1, 2019, pp. 245–274. doi:10.1007/s11831-017-9240-5.

[5] Yondo, R., Bobrowski, K., Andrés, E., and Valero, E., "A Review of Surrogate Modeling Techniques for Aerodynamic Analysis and Optimization: Current Limitations and Future Challenges in Industry," *Computational Methods in Applied Sciences*, Vol. 48, 2019, pp. 19–33. doi:10.1007/978-3-319-89988-6_2.

[6] Peherstorfer, B., Willcox, K., and Gunzburger, M., "Survey of multifidelity methods in uncertainty propagation, inference, and optimization," *SIAM Review*, Vol. 60, No. 3, 2018, pp. 550–591. doi:10.1137/16M1082469.

[7] Rasmussen, C. E., *Gaussian processes in machine learning*, Springer, 2003, pp. 63–71. doi:10.1007/978-3-540-28650-9_4.

[8] Rajabi, M. M., "Review and comparison of two meta-model-based uncertainty propagation analysis methods in groundwater applications: polynomial chaos expansion and Gaussian process emulation," *Stochastic Environmental Research and Risk Assessment*, Vol. 33, No. 2, 2019, pp. 607–631. doi:10.1007/s00477-018-1637-7.

[9] Ernst, O. G., Mugler, A., Starkloff, H. J., and Ullmann, E., "On the convergence of generalized polynomial chaos expansions," *ESAIM: Mathematical Modelling and Numerical Analysis*, Vol. 46, No. 2, 2012, pp. 317–339. doi:10.1051/m2an/2011045.

[10] Huyse, L., Stern, A., Pleming, J., Riha, D., Waldhart, C., and Thacker, B., "Verification of Stochastic Solutions Using Polynomial Chaos Expansions," *47th AIAA/ASME/ASCE/AHS/ASC Structures, Structural Dynamics, and Materials Conference*, 2006. doi:10.2514/6.2006-1994.

[11] Eldred, M., and Burkardt, J., "Comparison of non-intrusive polynomial chaos and stochastic collocation methods for uncertainty quantification," *47th AIAA aerospace sciences meeting including the new horizons forum and aerospace exposition*, 2009, p. 976. doi:10.2514/6.2009-976.

[12] Hosder, S., Walters, R., and Balch, M., *Efficient Sampling for Non-Intrusive Polynomial Chaos Applications with Multiple Uncertain Input Variables*, 2007. doi:10.2514/6.2007-1939, URL `https://arc.aiaa.org/doi/abs/10.2514/6.2007-1939`.

[13] Sargsyan, K., *Surrogate Models for Uncertainty Propagation and Sensitivity Analysis*, Springer International Publishing, 2016, pp. 1–26. doi:10.1007/978-3-319-11259-6_22-1.

[14] Blatman, G., and Sudret, B., "Sparse polynomial chaos expansions of vector-valued response quantities," *Safety, Reliability, Risk and Life-Cycle Performance of Structures and Infrastructures - Proceedings of the 11th International Conference on Structural Safety and Reliability, ICOSSAR 2013*, 2013, pp. 3245–3252. doi:10.1201/b16387-469.

[15] Kersaudy, P., Sudret, B., Varsier, N., Picon, O., and Wiart, J., "A new surrogate modeling technique combining Kriging and polynomial chaos expansions - Application to uncertainty analysis in computational dosimetry," *Journal of Computational Physics*, Vol. 286, 2015, pp. 103–117. doi:10.1016/j.jcp.2015.01.034.

[16] Shahzadi, G., and Soulaïmani, A., "Deep neural network and polynomial chaos expansion-based surrogate models for sensitivity and uncertainty propagation: An application to a rockfill dam," *Water (Switzerland)*, Vol. 13, No. 13, 2021. doi:10.3390/w13131830.

[17] Hosder, S., Walters, R., and Perez, R., *A Non-Intrusive Polynomial Chaos Method For Uncertainty Propagation in CFD Simulations*, 2006. doi:10.2514/6.2006-891.

[18] West, T. K., and Hosder, S., "Uncertainty quantification of hypersonic reentry flows with sparse sampling and stochastic expansions," *Journal of Spacecraft and Rockets*, Vol. 52, No. 1, 2015, pp. 120–133. doi:10.2514/1.A32947.

[19] West, T. K., Reuter, B. W., Walker, E. L., Kleb, B., and Park, M. A., "Uncertainty quantification and certification prediction of low-boom supersonic aircraft configurations," *Journal of Aircraft*, Vol. 54, No. 1, 2017, pp. 40–53. doi:10.2514/1.C033907.

[20] Rallabhandi, S. K., West, T. K., and Nielsen, E. J., "Uncertainty analysis and robust design of low-boom concepts using atmospheric adjoints," *Journal of Aircraft*, Vol. 54, No. 3, 2017, pp. 902–917. doi:10.2514/1.C033908.

[21] El Garroussi, S., Ricci, S., De Lozzo, M., Goutal, N., and Lucor, D., "Tackling random fields non-linearities with unsupervised clustering of polynomial chaos expansion in latent space: application to global sensitivity analysis of river flooding," *Stochastic Environmental Research and Risk Assessment*, 2021. doi:10.1007/s00477-021-02060-7.

[22] Benner, P., Gugercin, S., and Willcox, K., "A Survey of Projection-Based Model Reduction Methods for Parametric Dynamical Systems," *SIAM Review*, Vol. 57, No. 4, 2015, pp. 483–531. doi:10.1137/130932715.

[23] Brunton, S. L., Noack, B. R., and Koumoutsakos, P., "Machine Learning for Fluid Mechanics," *Annual Review of Fluid Mechanics*, Vol. 52, No. 1, 2020, pp. 477–508. doi:10.1146/annurev-fluid-010719-060214.

[24] Schmid, P. J., "Dynamic mode decomposition of numerical and experimental data," *Journal of Fluid Mechanics*, Vol. 656, 2010, pp. 5–28. doi:10.1017/S0022112010001217.

[25] Decker, K., Iyengar, N., Perron, C., Rajaram, D., and Mavris, D., *Nonlinear Multi-Fidelity Reduced Order Modeling Method using Manifold Alignment*, 2021. doi:10.2514/6.2021-3050.

[26] Iyengar, N., Rajaram, D., Decker, K., Perron, C., and Mavris, D. N., *Nonlinear Reduced Order Modeling using Domain Decomposition*, 2022. doi:10.2514/6.2022-1250.

[27] Decker, K., Iyengar, N., Rajaram, D., Perron, C., and Mavris, D., "Manifold Alignment-Based Nonintrusive and Nonlinear Multifidelity Reduced-Order Modeling," *AIAA Journal*, 2022, pp. 1–21. doi:10.2514/1.J061720.

[28] Raisee, M., Kumar, D., and Lacor, C., "A non-intrusive model reduction approach for polynomial chaos expansion using proper orthogonal decomposition," *International Journal for Numerical Methods in Engineering*, , No. March, 2015. doi:10.1002/nme.4900.

[29] Abraham, S., Tsirikoglou, P., Miranda, J., Lacor, C., Contino, F., and Ghorbaniasl, G., "Spectral representation of stochastic field data using sparse polynomial chaos expansions," *Journal of Computational Physics*, Vol. 367, 2018, pp. 109–120. doi:10.1016/j.jcp.2018.04.025.

[30] Li, G., Iskandarani, M., Hénaff, M. L., Winokur, J., Le Maître, O. P., and Knio, O. M., "Quantifying initial and wind forcing uncertainties in the Gulf of Mexico," *Computational Geosciences*, Vol. 20, No. 5, 2016, pp. 1133–1153. doi:10.1007/s10596-016-9581-4.

[31] El Moçayd, N., Shadi Mohamed, M., Ouazar, D., and Seaid, M., "Stochastic model reduction for polynomial chaos expansion of acoustic waves using proper orthogonal decomposition," *Reliability Engineering System Safety*, Vol. 195, 2020, p. 106733. doi:https://doi.org/10.1016/j.ress.2019.106733, URL `https://www.sciencedirect.com/science/article/pii/S0951832019303242`.

[32] Nagel, J. B., Rieckermann, J., and Sudret, B., "Principal component analysis and sparse polynomial chaos expansions for global sensitivity analysis and model calibration: Application to urban drainage simulation," *Reliability Engineering System Safety*, Vol. 195, 2020, p. 106737. doi:https://doi.org/10.1016/j.ress.2019.106737.

[33] "Random dynamical system in time domain: A POD-PC model," *Mechanical Systems and Signal Processing*, Vol. 133, 2019, p. 106251. doi:10.1016/j.ymssp.2019.106251.

[34] Bishop, C. M., *Pattern Recognition and Machine Learning (Information Science and Statistics)*, Springer-Verlag, Berlin, Heidelberg, 2006.

[35] Kerschen, G., et al., "The Method of Proper Orthogonal Decompostion for Dynamical Characterization and Order Reduction of Mechanical Systems: An Overview," *Nonlinear Dynamics*, Vol. 41, No. 1-3, 2005, pp. 147–169. doi:10.1007/s11071-005-2803-2.

[36] Sirovich, L., "Turbiulence and the Dynamics of Coherent Structures: Part I: Coherent Structures," *Quarterly of Applied Mathematics*, Vol. XLV, No. 3, 1987, pp. 561–571.

[37] Wiener, N., "The homogeneous chaos," *American Journal of Mathematics*, Vol. 60, No. 4, 1938, pp. 897–936.

[38] Xiu, D., and Karniadakis, G. E., "The Wiener–Askey Polynomial Chaos for Stochastic Differential Equations," *SIAM Journal on Scientific Computing*, Vol. 24, No. 2, 2002, pp. 619–644. doi:10.1137/S1064827501387826.

[39] Eldred, M., Webster, C., and Constantine, P., *Evaluation of Non-Intrusive Approaches for Wiener-Askey Generalized Polynomial Chaos*, 2008. doi:10.2514/6.2008-1892.

[40] Najm, H. N., "Uncertainty quantification and polynomial chaos techniques in computational fluid dynamics," *Annual Review of Fluid Mechanics*, Vol. 41, 2009, pp. 35–52. doi:10.1146/annurev.fluid.010908.165248.

[41] Poëtte, G., "A comparative study of generalized Polynomial Chaos based Approximations: integration vs. regression vs. collocation vs. kriging," 2018.

[42] Iyengar, N., Mavris, D., and Rajaram, D., "Uncertainty Propagation in CFD Simulations using Non-Intrusive Polynomial Chaos Expansion and Reduced Order Modeling," *Bulletin of the American Physical Society*, 2022.

[43] Lin, G., Su, C. H., and Karniadakis, G. E., "Predicting shock dynamics in the presence of uncertainties," *Journal of Computational Physics*, Vol. 217, No. 1, 2006, pp. 260–276. doi:10.1016/j.jcp.2006.02.009.

[44] Sederberg, T. W., and Parry, S. R., "Free-form deformation of solid geometric models," *Proceedings of the 13th annual conference on Computer graphics and interactive techniques*, 1986, pp. 151–160.